Physics Engineering
Bachelor's Thesis

Study of the relaxation behaviour of severely deformed bulk metallic glasses

Author: Anna Girbau
Director: Prof. Dr. Gerhard Wilde
Codirector: Prof. Dr. Jordi Llorca
Supervisor: Mark Stringe

Institute of Material Physics - Wilde Group (WWU-Münster)

January 2019

UNIVERSITAT POLITÈCNICA
DE CATALUNYA
BARCELONATECH

Contents

List of abbreviations and variables

BMG	Bulk Metallic Glass
DSC	Differential Scanning Calorimetry
GFA	Glass Forming Ability
HPT	High Pressure Torsion
HP	High Pressure
HPT5	High Pressure Torsion (5 rotations)
MRO	Medium Range Order
XRD	X-Ray Diffraction
R_c	Critical cooling rate
T_f	Fictive temperature
T_g	Glass transition temperature
T_l	Liquidus temperature
T_m	Melting temperature
T_{rg}	Reduced glass transition temperature
T_x	Crystallisation temperature
τ	Relaxation time
ΔH_x	Crystallisation enthalpy
ΔH_{relax1}	Relaxation enthalpy (1st cycle)
ΔH_{relax2}	Relaxation enthalpy (2nd cycle)
ΔP	Power difference
Φ	Heat flow
β	Heating rate
η	Viscosity

Abstract

Glasses have been used by people for years and represent an important class of materials, which today are an indispensable part of everyday life. In order to produce a metallic glass, the amorphous melt must be cooled down so quickly that the crystallisation cannot take place. If this succeeds, the amorphous state can be frozen and the metallic glass will have a disordered structure.

Metallic glasses are characterised by a high hardness, corrosion resistance, a high elastic limit and good soft magnetic properties. However, metallic glasses have the great disadvantage that they show almost no plastic area. The project consists in studying the relaxation behaviour of a Pd-based alloy, which is the exothermic signal appearing before glass transition, when it is severely deformed by high pressure torsion (HPT). Some indicators manifest that during the relaxation process exothermic events can appear, due to alpha and beta relaxation; these signals will be more or less noticeable depending on the heating rate and the type of deformation applied.

The aim is to analyze why these calorimetric signals, which indicate the presence of different relaxation mechanisms that show different sensitivities concerning to the applied pressure (8 GPa) and 5 rotations with the HPT, appear in the relaxation process. Differential Scanning Calorimetry (DSC) and Kissinger analyses shall be employed to determine the activation energies of these peaks, in order to discuss their physical origin and relate them with their corresponding relaxation type.

1 Introduction

Amorphous metals differ from common metallic alloys through the absence of the cystalline long-range order and the associated translational symmetry. A glass is defined as an amorphous solid showing a glass transition. In order to reach the glass state, a continued cooling must be applied avoiding nucleation of the crystalline structure by quenching a melt, since the material reaches a metastable supercooled liquid and achieves the glass state. To avoid crystallization, the so called crystallization-nose in a TTT (Time temperature transformation) diagram must be bypassed.[1]

In contrast to crystalline materials, amorphous metals do not possess crystal defects such as grain boundaries, dislocations or precipitates of other phases. The atomic structure obtained by the glass formation leads to interesting properties, e.g. corrosion resistance due to the lack of grain boundaries, high hardness, high strength and pronounced elasticity [7]. Currently, the response of external mechanical stresses applied to the metallic glasses leading to elastic or plastic strain is a topic of high interest, since the absence of a crystal lattice necessitates the existence of accommodation mechanisms that are not based on dislocations or grain boundaries, as in crystalline materials. In fact, it is now accepted that yielding of metallic glasses starts in a highly localized fashion, involving regions of a few tens of atoms only. Upon continued straining, mesoscopic and plate-like defects, so-called shear bands form that accommodate localized plastic flow and at the same time cause work softening that often leads to catastrophic failure. So far, only little is known about the properties of these shear bands and how they are formed, evolve and interact.

In this project, the main objective is to analyze the relaxation behaviour, which occurs before the glass transition, of a Pd-based alloy after severely deforming the sample by HPT (High Pressure Torsion). There are some indicators which manifest that during the relaxation process some exothermic events can appear, due to relaxation[2]; these events are more or less noticeable depending on the heating rate of calorimetric measurements. In conclusion, the aim of this project is to analyze the origin of these calorimetric signals that indicate the presence of different relaxation mechanisms that show different sensitivities concerning to the applied pressure (8 GPa) and 5 rotations with the HPT. Calorimetry and Kissinger analyses shall be employed to determine the activation energies of these peaks so that their physical origin can be discussed.

[1] Section 2.1.4
[2] Section 2.1.5

2 Theoretical fundamentals

2.1 Metallic glasses

A metallic glass can be defined as a kind of frozen liquid with small free volume and high viscosity (in comparison with the liquid viscosity), which bypass somehow the nucleation of the crystalline phase [26]. Amorphous metal alloys are glass forming at specific cooling rates in the bulk via conventional metal processing such as casting, but with the ease of molding of polymers. When a conventional metal or alloy cools from the liquid melt, equilibrium is reached when it solidifies into the lowest energy state structure. In industrial environments, metals crystallize at temperatures just below the melting point in microseconds. A glass has such slow crystal nucleation and growth kinetics that the liquid can be undercooled far below its melting point before a glass transition is reached during 'freezing,' which as a vitreous solid without crystallizing occurs. Glass is brittle, even though the atoms retain an amorphous distribution. They show high strength, have greater wear and corrosion resistance, are tougher than ceramics, and yet have greater elasticity [21]. Most metals are polycrystalline with grains of varying shapes and sizes; forming a perfect single crystal is not probable. Under sufficient stress and heat, misaligned planes of atoms slip past each other easily, allowing dislocations to move. As a result, metals have a much lower strength than their theoretical maximum and deformation is plastic and permanent, due to the energy going into moving atoms out of the way.

2.1.1 Classes of amorphous metals

Metallic glasses are formed by two or more atomic components. It is not yet possible to transfer elementary metals by rapid quenching of the melt into the amorphous state. At relatively low temperatures glass-forming alloy systems often have eutectic[3] points in the equilibrium phase diagram. This means that the melt is stable up to relatively low temperatures.

According to their composition, the classes of amorphous metals can be distinguished as it follows:

- **Metal-metalloid-glasses** consist mostly of late transition metals (Fe, Ni, Co, ...) and a metalloid[4] element (B, P, ...) of about 20 atomic percent. The smaller metal-

[3]Homogeneous mixture of substances that melts or solidifies at a single temperature that is lower than the melting point of either of the constituents.

[4]A nonmetal that in combination with a metal forms an alloy

loid atom acts as a glass former and hinders the formation of a crystalline structure during quenching of the melt.

- Amorphous metals form **alloys of early and late transition metals** (Co-Zr, Ni-Nb, ...)
- **Bulk metallic glasses** are multicomponent alloys with a high glass-forming ability, which is comparable to that of silicate glasses. Melts of such materials can be solidified glassy even at relatively low cooling rates (1 to 100 K per second), which is achieved with normal casting operations. One can therefore not only produce thin ribbons but also bulk metallic glasses.

This work will be focused on the third class concerning bulk metallic glasses.

2.1.2 Properties and structure of amorphous metals

As well as crystalline alloys, amorphous metals present metallic conductivity and to a certain extent metallic ductility. The fact that the metallic glasses have an amorphous structure and present no crystal defects causes often favorable properties: Metallic glasses are among the materials with extremely high hardness (for surface coatings) and strength without dislocations. A very high elastic limit is presented because of its high yield strength. The elastic (Hooke) range in the stress-strain curve has a large expansion, therefore, a high amount of elastic energy is stored. These material also present high toughness (more fracture resistant than ceramics) [21].

The studied material is $Pd_{40}Ni_{40}P_{20}$ (at. %). When the material is characterized with the differential scanning calorimetry (DSC), the following temperatures and heat flow should be obtained (Table 2.1) in order to know that the sample is behaving as expected[5].

Composition	T_g (°C)	T_m (°C)	T_x (°C)	$\Delta T_x = T_x - T_g$ (°C)	ΔH_x (kJ/mol)
$Pd_{40}Ni_{40}P_{20}$	303	604	405	102	7.37

Table 2.1: T_g, T_m, T_x, ΔT_x, ΔH_x of PdNiP (BMG) determined by DSC at a scanning rate of 20K/min [27] [26]

[5]Section 3.4

Amorphous solids have a certain short-range order[6] of atoms and no translational symmetry in contrast to crystals. The structure of a metallic glass can be described as a random packing of spheres as can be seen in figure 2.1.

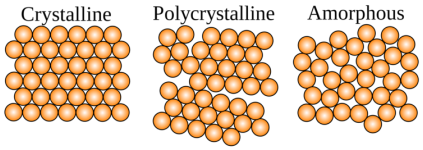

Figure 2.1: Structures of monocrystalline, polycrystalline and amorphous metal [17]

2.1.3 Glass-forming ability (GFA)

The glass-forming ability (GFA) is defined as the easiness of vitrification, which is important for understanding the origin of glass formation, for the design and synthesis of BMG, and the resistance to crystallisation of the glass. A perfect definition of GFA should include the glass forming tendency of the liquid and the thermal stability of the glass [3].

GFA is normally quantified by the critical cooling rate (R_c) and the maximum section thickness or diameter (Z_{max}) and it is accepted that GFA is proportional to T_x/T_g and T_g/T_l [3].

Some of the criteria proposed for GFA calculation are the following ones [3] [26]:

$$T_{rg} = T_g/T_l \qquad \Delta T_x = T_x - T_g \qquad \gamma = T_x/(T_g + T_l)$$
$$\beta = T_x/T_g + T_g/T_l \qquad \gamma_m = (2T_x - T_g)/T_l \qquad \delta = T_x/(T_l - T_g)$$
$$\Phi = T_{rg}(\Delta T_x/T_g)^{0.143} \qquad \beta_1 = (T_x \cdot T_g)/(T_l - T_x)^2 \qquad \omega = T_g/T_x - 2T_g/(T_g + T_l)$$

These values can be calculated easily with the parameters of table 2.1.

The reduced glass transition temperature (T_{rg}), can be used to determine the GFA of an alloy. If the relation $T_{rg} = T_g/T_m = 2/3$ is accomplished will mean that the crystallisation can happen in a very narrow temperature range; in consequence, the liquid can be easily undercooled at a low cooling rate into a glass [26]. One of the principles that should be taken into account when designing BMG alloys is picking elements with different sizes; this will lead to a complex structure which will be less easy to crystallise, and take into account compositions with deep eutectics that will form liquids stable at low temperatures. The "confusion principle" explains that, in general, the GFA in BMGs has a tendency to increase when more components are added to the alloy, due to the destabilisation of

[6]Refers to the regular and predictable arrangement of atoms over a short distance, usually with one or two atom spacings. However, this regularity does not persist over a long distance. [6]

the system making the crystalline phases compete with each other during cooling, which implies that the melting process will be more stable [26].

In the case of $Pd_{40}Ni_{40}P_{20}$ the reduced glass transition temperature is 0.66 which is almost the ideal result 2/3 from the GFA.

$$T_{rg} = \frac{T_g}{T_m} = \frac{303 + 273}{604 + 273} = 0.66$$

2.1.4 TTT Diagram (Time Temperature Transformation diagram)

The TTT diagram (figure 2.2) is the representation of the information to predict the formability and stability of the glasses. It is useful to describe the glass formation kinetics. By this diagram, one can determine physical and thermal properties such as heat capacity. [21]

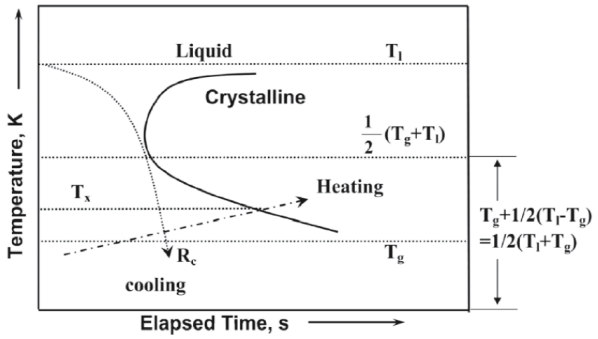

Figure 2.2: TTT diagram for a metallic glass [20]

Crystallization occurs between T_l and T_g and can be avoided with a sufficient cooling rate larger than the critical cooling rate (R_c). When heating, the sample starts to crystallize at an onset temperature denoted as T_x, which will depend on the heating rate. [20] Holding isothermally at temperatures above T_g will also lead to different T_x in dependence of the isothermal temperature.

The "nose" shape is due to the competing interplay between the increasing driving force of the sample to crystallize and the effective diffusivity[7] of the atoms [26].

[7]Slowing down of kinetics

2.1.5 Relaxation process

The relaxation is determined by the movement of the atoms in different modes, and its corresponding relaxation times τ are the times needed to reach energetically the most favourable state of the atoms. The slow relaxation towards equilibrium is commonly referred to as physical aging, its effects can be eased by heating above glass transition temperature [12]. During the relaxation process rejuvenation or aging can occur, if the heat flow signal (Endo Up) is shifted down will mean that aging is happening, and if is shifted up rejuvenation is taking place. It is common to distinguish between two different relaxation mechanisms in metallic glasses which are α- and β- relaxation.

α-RELAXATION

The α-relaxation, also known as structural relaxation, occurs when the alloy is warmed up (annealed) to a temperature below T_g, the structure relaxes slowly and its T_f and the volume come down. This phenomenon is called structural relaxation. The greater the structural disorder and the free volume, the exothermic energy release is more pronounced due to structural relaxation at the beginning of the glass transition [20].
The α-relaxation is usually associated with atomic motions within clusters of atoms and often can be reversible. These process is slower than the β-relaxation one.

β-RELAXATION

The β-relaxation corresponds to the motion of clusters or atomic transport between clusters [4]. It occurs at lower temperatures because it does not need so much energy to happen.

2.2 High Pressure Torsion (HPT)

The technique used to deform severely the samples is High Pressure Torsion (HPT). The HPT device works by introducing strain into a sample as shown in figure 2.3, this leads crystalline materials to a grain size reduction so the material will be harder. As it can be seen, the sample is placed between two anvils with the same diameter as the sample (ϕ $5mm$) and a compressive stress of 8 GPa (HP) is applied, afterwards, to study the difference between a sample with applied rotations and without, a five-rotation process (HPT5) is applied rotating the anvil above and maintaining the other one without any movement. Each rotation lasts approximately 1 minute and 7 seconds.

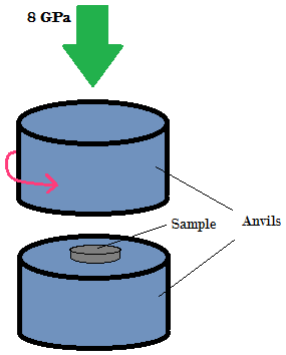

Figure 2.3: HPT. *Pressure applied* $= 8\ GPa$. The lower anvil remains fixed while the upper rotates.

In order to calculate the strain value the following formula can be used [18]:

$$\gamma = \frac{2\pi \cdot R \cdot N}{l} \tag{1}$$

To calculate the shear strain value at a distance R from the axis of the disk type sample the equation (1) is used in the case of usual torsion straining with the following parameters:
N: Number of rotations
l: Thickness of the sample
R: Radius of the sample

2.3 Differential scanning calorimetry (DSC)

A differential scanning calorimeter (DSC) is a thermoanalytical device in which the difference in the amount of heat required to increase the temperature of a sample compared to a reference can be measured. Both are encapsulated in aluminum crucibles whereas the reference is an empty crucible. One can investigate the enthalpy, the heat capacity and other parameters.
Two types of DSCs can be distinguished:

- The **power compensating DSC** which measures the power difference.
- The **heat flux DSC** which measures the temperature difference

In this project the samples will be studied by the power compensating DSC, which works as shown in figure 2.4.

In the power difference calorimeter, the sample and the reference are located in two different furnaces which are heated separately. The power which is needed to keep the two ovens at the same temperature is measured. The following relation results from the power difference ΔP:

$$\Delta P = -k_1 \cdot \Delta T \tag{2}$$

$$\Phi = -k_2 \cdot \Delta T \tag{3}$$

The heat flow (Φ) is defined by the exchange of heat between two crucibles (Figure 2.4). The measured signal is given as a heat flow, which is obtained by a proportionality of the temperature difference, caused by thermal asymmetries like phase transformations of the sample and reference furnaces upon scanning with a certain temperature program. The aim is to compensate this thermal asymmetries with a differential power applied to the sample and reference respectively in a way that ΔT is minimized. The calibration factors of the device are k_1 and k_2.

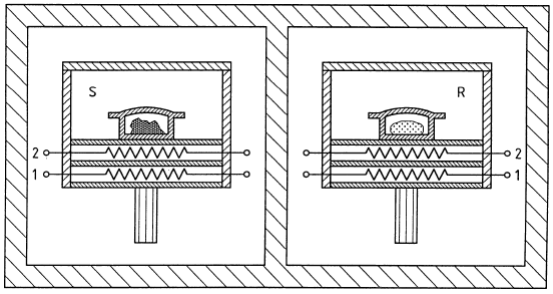

Figure 2.4: Setup of the power compensating DSC. 1-Heating wire, 2-Resistance thermometer. S-Crucible with sample, R-Crucible with the reference sample. [8]

Both measuring systems are separated from each other and positioned in a surrounding (block) at constant temperature.

2.4 X-Ray Diffraction (XRD)

Diffraction effects are observed if electromagnetic radiation encounters an obstacle whose size is the length scale of the radiation wavelength. The interatomic distances of the studied materials are in the range of some Angströms, which corresponds to the wavelength of X-rays. Consequently, X-ray (XRD) diffraction can be used to study the structure of

materials to know if the studied samples are glasses or crystals.

Let us consider a simple cubic lattice. The distance between two adjacent planes is given by d_{hkl} with the Miller indexes of the appropriate lattice planes. For cubic lattices the interplanar spacing depends on the lattice constant a and the Miller indexes according to:

$$d_{hkl} = \frac{a}{\sqrt{h^2 + k^2 + l^2}} \tag{4}$$

If Bragg's law (5) is satisfied there is a constructive interference, this implies having a maximum intensity in the diffraction pattern as observed in equation (4).
The experimental methods which can be used are:

1. Debye-Scherrer method

2. Laue method

In this case the sample will be studied with the Debye-Scherrer method. For crystalline materials, rings whose locations are determined by the Bragg condition are expected because of the reflection of monochromatic X-rays at the lattice planes of the crystallites. In an X-ray analyses this corresponds to sharp peaks where the Bragg's condition is fullfilled.

When the sample is irradiated with plane wave X-rays, in this case the K_α radiation from Copper with a wavelength of $\lambda = 1.541\mathring{A}$, a set of crystallographic lattice planes with distances d_{hkl} is irradiated by hitting on the lattice planes at an angle θ. The relative phase shift of the scattered wave depends on the configuration of atoms. Hence, each material will have a set of characteristic peaks in the diffraction pattern if the presented material is a crystal, which allows to determine the different phases present in a sample and helps to determine the crystal structure.

A lack of crystalline structure can be detected, because there are some broad peaks appearing caused by the presence of a short-range order, indicating that the nearest neighbours of an atom are preferably located in a mean distance $\overline{d}$. This distance can be determined by the Bragg equation of the angular position $\overline{\theta}$ of the maxima of a diffractogram:

$$2 \cdot \overline{d} \cdot \sin \overline{\theta} = \lambda \tag{5}$$

In the studied case, if the peaks appear will mean that the samples need to be done again because they are not completely amorphous.

3 Experimental part

3.1 Sample process

In order to carry out the proposed experiments, the samples were produced following the steps explained below.

First of all, to fabricate the $Pd_{40}Ni_{40}P_{20}$ samples with the corresponding proportions 40-40-20 (at %), it is necessary to weight the quantity of each element so the alloy can be created. As said in section 2.2, the samples need to have a diameter of 5 mm in order to fit with the HPT device; that is the reason why the samples are produced in a cylinder shape and, afterwards, cut in pieces which are parallel to the base. The desired cylinder that fits inside the mold weights about 5 g, in consequence, it is necessary to adjust the proportions (40-40-20) to the weight of the sample. The proportions are calculated with the alloy calculator as it can be seen in figure 3.1:

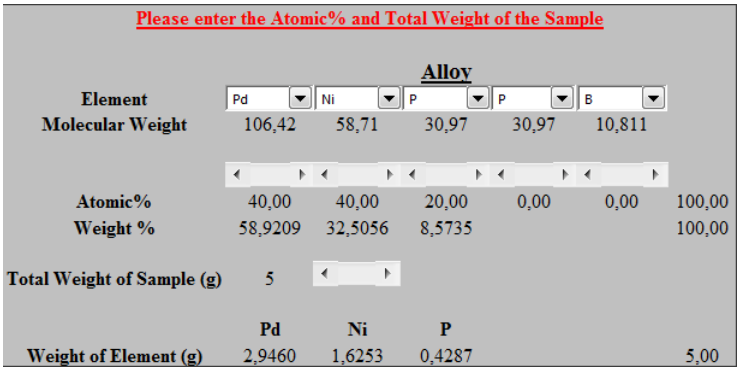

Figure 3.1: Alloy calculator for $Pd_{40}Ni_{40}P_{20}$

Figure 3.1 shows the quantities which must be measured to form the 5 g $Pd_{40}Ni_{40}P_{20}$ alloy, having then 2.9460 g of Pd, 1.6253 g of Ni and 0.4287 g of P.

Due to the instability of the P and Ni, they will be weighted as Ni_2P molecule which follow the desired proportions for the alloy $Pd_{40}Ni_{40}P_{20}$; then the needed mass is the sum of both Ni and P having then 2.0540 g of Ni_2P.

The measured values are presented in table 3.1:

Pd	Ni_2P
2945.96 mg	2054.03 mg

Table 3.1: Weighted elements of the $Pd_{40}Ni_{40}P_{20}$ alloy (in mg)

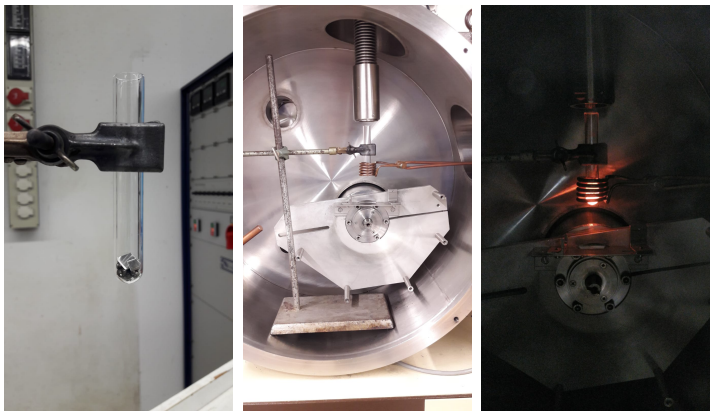

Figure 3.2: $Pd_{40}Ni_{40}P_{20}$ before and while melting held in a ring stand

Figure 3.2 shows the weighted elements inside a test tube held in a ring stand so it can be introduced to the melt-spinning device.

After putting the ring stand with the sample inside the melt-spinning device and before the melting process, the vacuum needs to be created inside the chamber. When the melt-spinning device starts working the current travels through the copper coil heating the sample.

First of all, the sample needs to be pre-melted following the next process: the turbo-pump is switched on in order to reach a pressure of $10^{-6}Pa$, after that, the argon gas is introduced into the chamber so the sample is melted in an argon atmosphere.

The argon gas is used because it is heavier than air and it is a noble gas, which does not react with metals and acts like a cleaning agent; when fabricating a sample the oxygen needs to be removed. When the argon gas is spread over the atmosphere the current is gradually raised in the coil with a rate of 0.3 A/min waiting for the signal of the temperature to raise until it reaches more or less $1100°C$, which is around the melting temperature (T_m) of $Pd_{40}Ni_{40}P_{20}$ ($1150.3°C$ [26]). As the melting temperature is reached, so the alloy is formed, one needs to cool again the coil with a rate of 0.5 A/min until 2.8 A and then turn off the device.

Figure 3.3: Sample prepared with acetone for the ultrasonic bath

The pre-melting process results in a little ball as shown in figure 3.3. The $Pd_{40}Ni_{40}P_{20}$ alloy is placed inside a beaker with acetone so it can be brought into the ultrasonic bath[a], in order to take out the boron oxide obtained from the pre-melting process, which is used because the oxid of the surface of the samples needs to be removed.

[a]Ultrasonic cleaning is a process that consists in agitating a fluid using ultrasound ($\sim$ 20–400KHz).

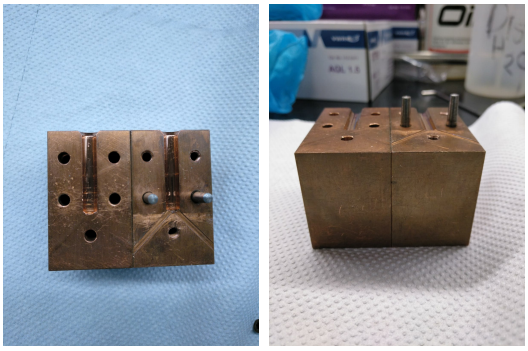

Figure 3.4: Copper mold (∅5)

Figure 3.4 presents the copper mold used to fabricate the $Pd_{40}Ni_{40}P_{20}$ sample, the diameter of the mold is 5 mm. The copper mold dimensions are the presented ones because the sample must fit in the anvils of the HPT and in the crucibles of the DSC. After obtaining the sample, it will be cut with the wiresaw device, obtaining then a huge amount of samples from the $Pd_{40}Ni_{40}P_{20}$ alloy cylinder.

The copper mold and the sample with its corresponding glass tube are placed inside the melt-spinner aligned in such a way that the alloy can be introduced inside the copper mold as shown in figure 3.5.

Finally, the last step that needs to be done before using the wiresaw device is polishing the whole sample with polish papers from rougher to finer which are: P1200, P2500, P4000. These values correspond to particle sizes of 15 μm, 10 μm and 5 μm. The polishing process is necessary to remove possible oxidation from the surface of the sample.

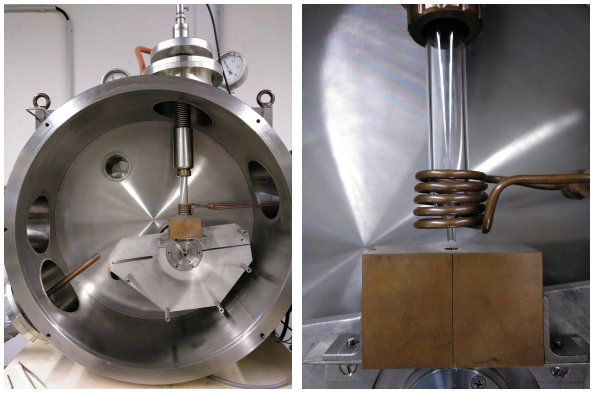

Figure 3.5: Copper mold introduced in the melt spinner device

3.2 XRD of the sample

In order to confirm that the $Pd_{40}Ni_{40}P_{20}$ alloy is a metallic glass or if the solid has got a crystalline structure, the whole sample is cut into pieces with the wiresaw obtaining samples with a certain height. This sample is introduced in the X-Ray diffraction device with the program shown in figure 3.6, the obtained results can be observed in figure 3.7 with their corresponding gaussian approximations over the two peaks.

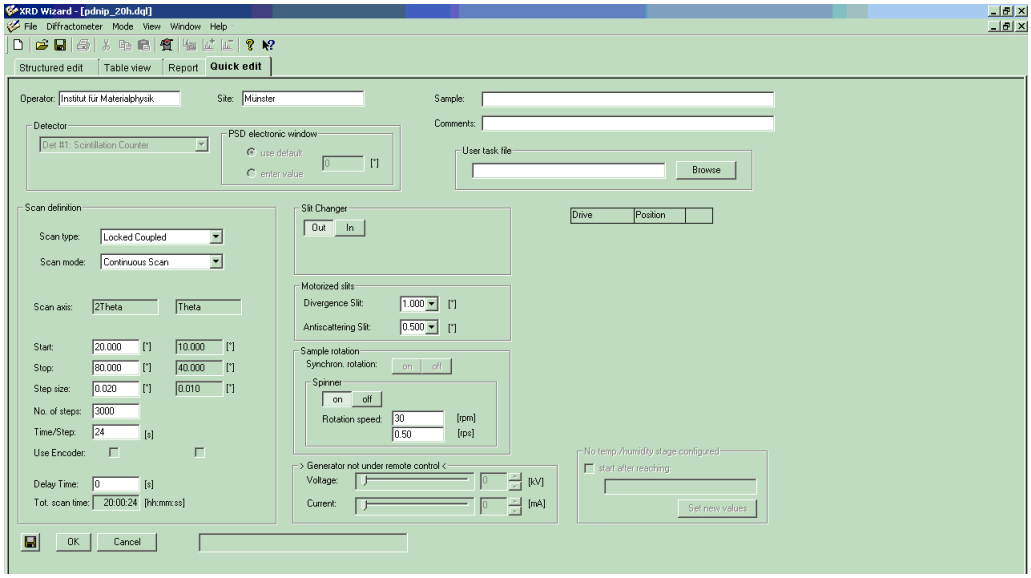

Figure 3.6: XRD program used to prove the presence of metallic glass

Figure 3.6 shows different parameters used to analyse the alloy. The start and the stop parameters indicate where the measurement starts and ends. The step size indicates that along 1° 50 steps are done, consequently, the number of steps is an automatic parameter given by the program which depends on the step size and the range that the XRD device has to measure. Finally, the Time/Step indicates that every 0.020° the program stops 24 seconds, this is the reason why the total scanning time is roughly 20 hours.

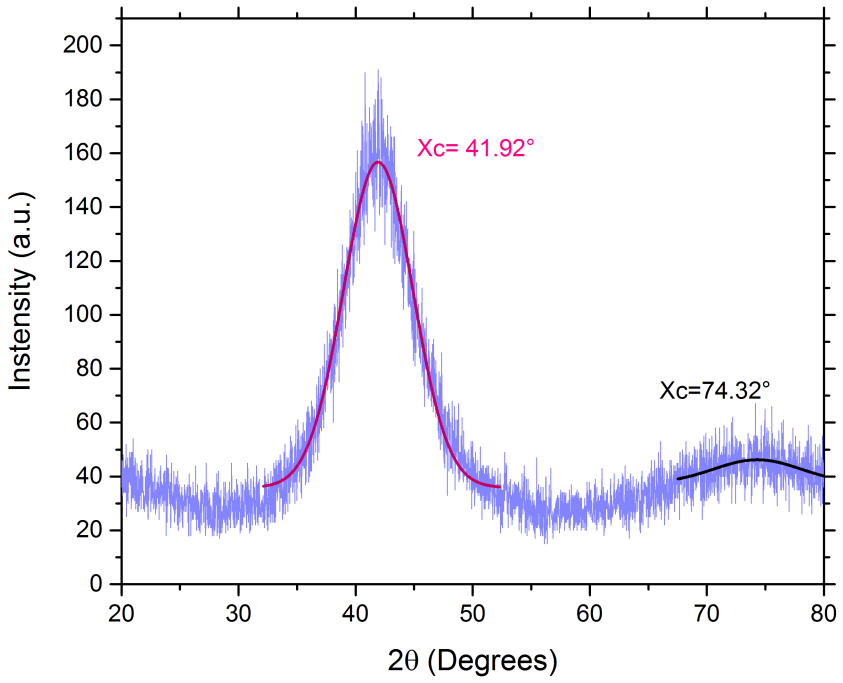

Figure 3.7: Intensity (a.u.) vs. 2θ (Degrees) - XRD of $Pd_{40}Ni_{40}P_{20}$

Figure 3.7 shows the representation of the intensity vs. 2θ and their respective angles' values in which the intensity peaks are found. They are useful to calculate the nearest neighbours' distance applying the equation (5) obtaining the following results:

Sample	$\theta_1(^\circ)$	$d_1(\mathring{A})$	$\theta_2(^\circ)$	$d_2(\mathring{A})$
$Pd_{40}Ni_{40}P_{20}$	41.92	2.15	74.32	1.28

Table 3.2: Nearest neighbours' distances d_1 and d_2 and their respective angle θ

Table 3.2. show the different distances between atoms. Knowing that Pd has got a radius of 1.79 $\mathring{A}$, Ni of 1.62 $\mathring{A}$ and P of 1.23 $\mathring{A}$ [16]; one can compare the radius of the elements from the alloy with the nearest neighbours' distances and confirm that the order of magnitude is the same.

3.3 Illustrated calculations for parameters

The structure changing of the materials occurs faster at high temperatures and at low temperatures the change slows down. Below a certain temperature, the structure appears to be frozen because of "kinetic arrest". This temperature is the glass transition temperature (T_g). When a liquid is cooled rapidly, this kinetic arrest occurs when the temperature is higher, and the system freezes above Tg (dashed line in Fig. 3.8). The temperature at which the thermal arrest happens is called the fictive temperature (T_f) of that state. [20]

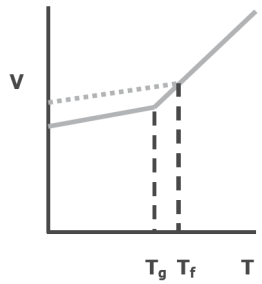

Figure 3.8: Volume vs. temperature with slow (solid line) and fast (dashed line) cooling from the liquid [19]

$\underline{T_{g1/2}}$

The glass transition Temperature can be calculated in several ways, in this project it is calculated by the following method:

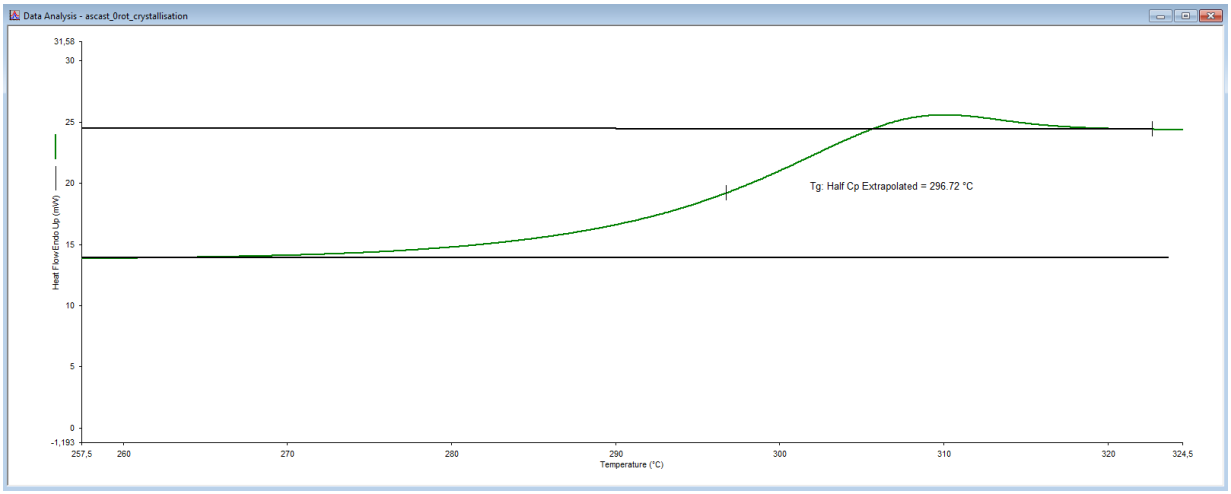

Figure 3.9: Glass transition temperature ($T_{g1/2}$) calculation

$\underline{T_f}$

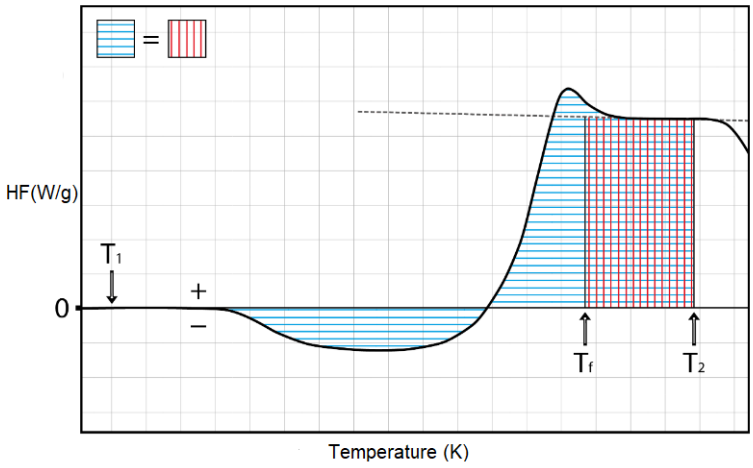

Figure 3.10: Fictive temperature T_f calculation [22]

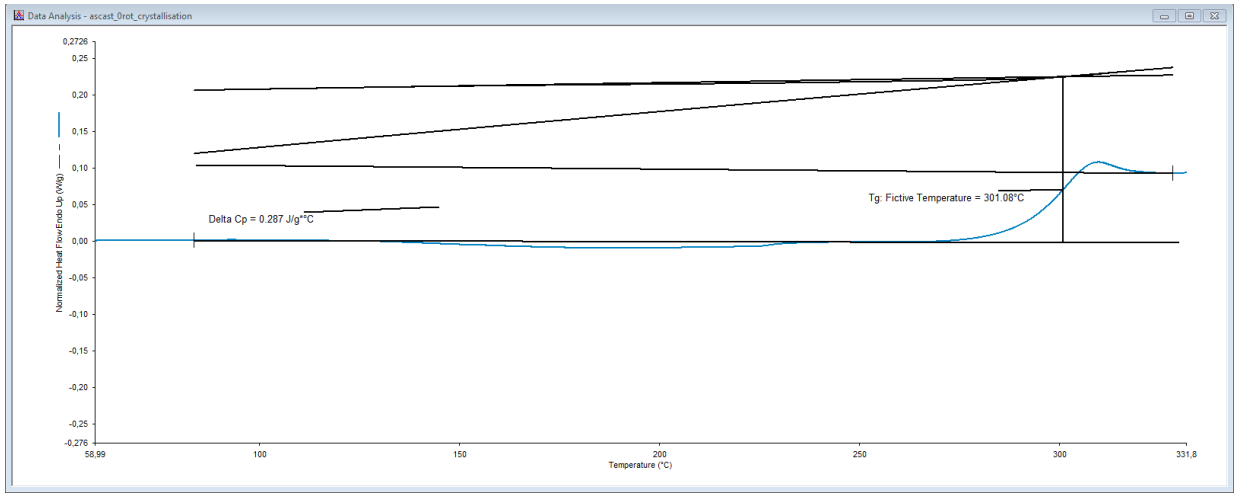

Figure 3.11: T_f calculation with the Pyris program

T_x

Figure 3.12 corresponds to the mean value of the crystallisation temperature.

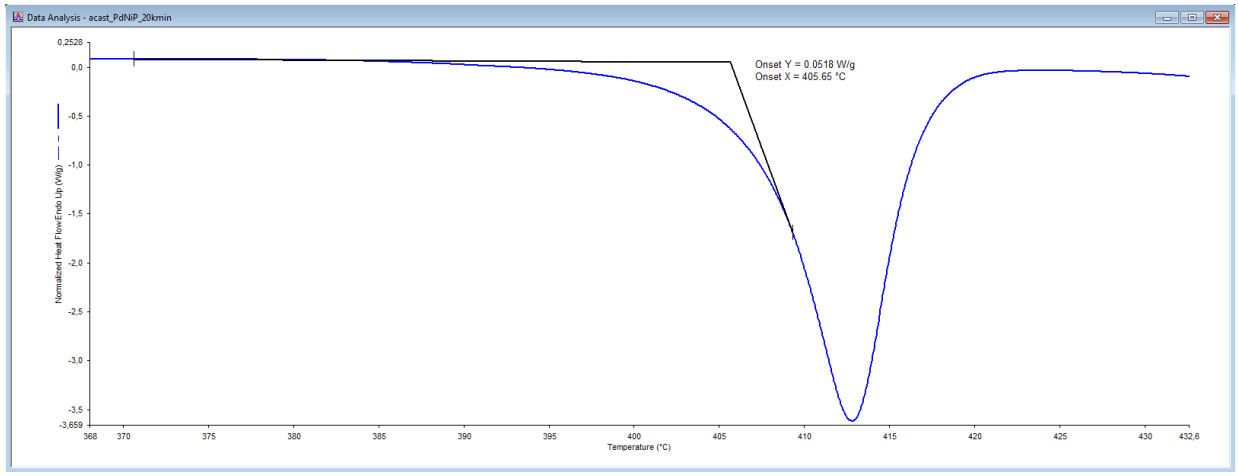

Figure 3.12: Crystallisation temperature (T_x) calculation

ΔH

The variation of enthalpy is described as (6) obtaining then a value with units of J/g.

$$\Delta H = \frac{A}{\beta \cdot m} \tag{6}$$

Being A the area (7), β the heating rate, Φ the heat flow and m the mass of the sample.

$$A = \int_{T_1}^{T_2} \Phi \cdot dT \tag{7}$$

Reference states

- **Baseline:**
  The baseline is the result of measuring the heat flow of two empty crucibles for every heating rate, afterwards the 3rd heating step of the baseline measurement is selected and subtracted to the different heating steps, in a way that it is only taken into account the signal from the studied sample. Figure 3.13 shows in red all the heating and cooling steps from the measurement and in blue the last heating step, which is the one subtracted to all of the heating cycles after each measurement, in order to erase the signal contribution from the device.

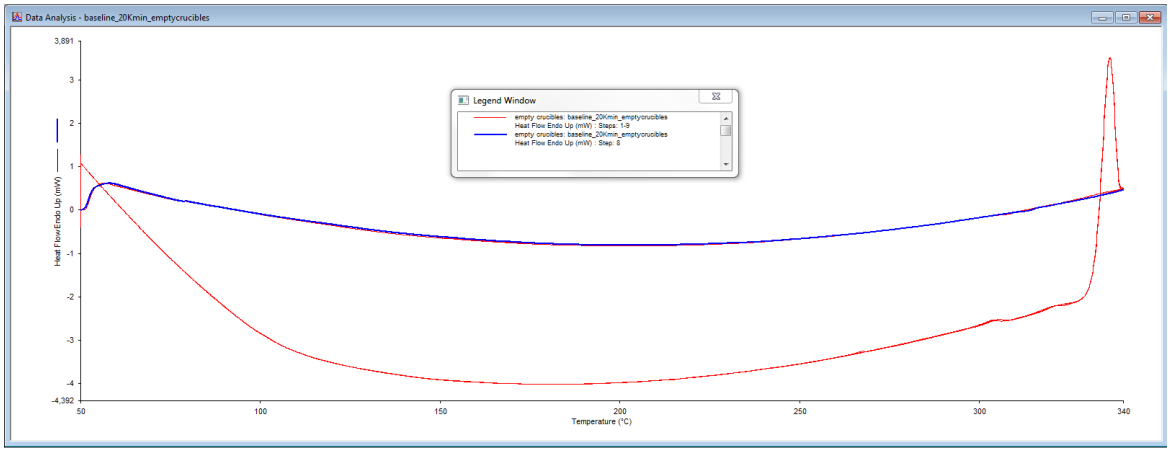

Figure 3.13: Heat flow vs. Temperature from two empty crucibles at a heating rate of 20 K/min.

These baseline is used when studying one heating cycle. When analysing the subtraction between cycles it is not necessary to subtract the baseline because it is included in the process, if not the baseline would be subtracted twice.

- **Reference state at a heating and cooling rate of 20 K/min:**
  In section 4.1. the cooling rates are studied and the reference state of the heating steps is the heating curve at 20 K/min. This means that the heating step, after being

cooled at 20 K/min, is subtracted to all of the heating steps after their corresponding cooling step at a certain cooling rate. Subtracting the first and the second steps one can obtain a 0 line result, showing that the reproducibility of the samples is good as shown in figure 3.14.

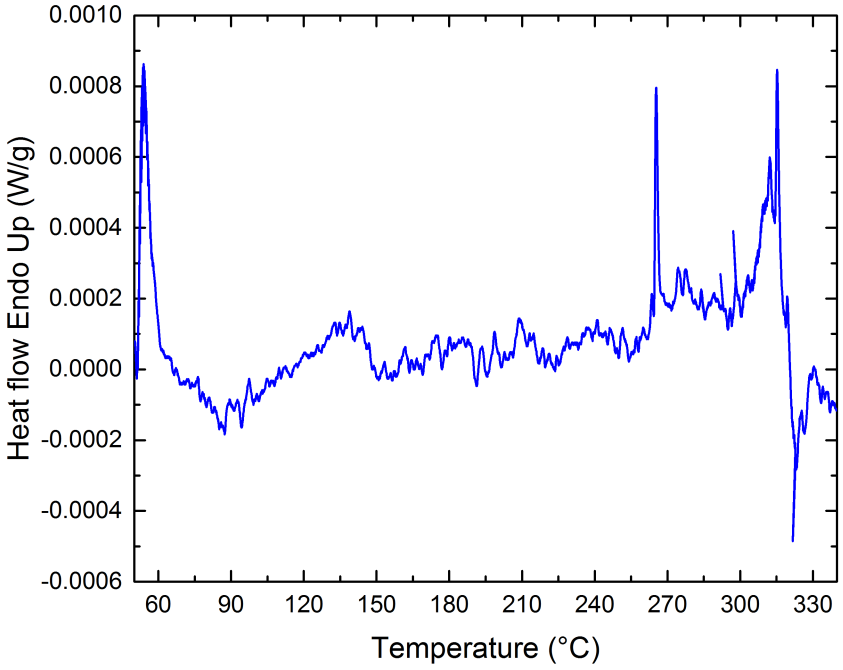

Figure 3.14: Subtraction of two heating steps at 20 K/min

3.4 Sample characterization

After cooling the system, calibrating the DSC and preheating the device, the $Pd_{40}Ni_{40}P_{20}$ sample is introduced into the DSC in order to make a first measurement of the material as shown in figure 3.15. The DSC is calibrated by taking a sample of indium and lead, measuring their corresponding melting temperatures and introducing the values in the device so it compares the experimental value and the theoretical one.

The normalization in all the cases is done by dividing the signal by the corresponding sample mass.

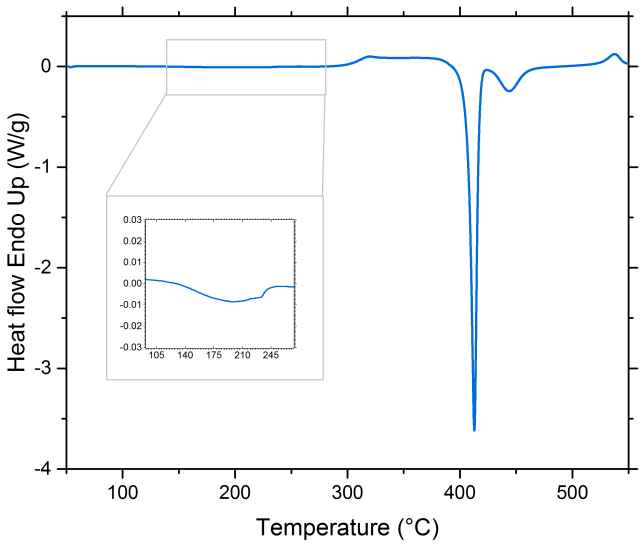

Figure 3.15: Normalized Heat flow of $Pd_{40}Ni_{40}P_{20}$ as cast at 20 K/min

In figure 3.15 the heat flow of $Pd_{40}Ni_{40}P_{20}$ is represented with the DSC showing the different transitions of the material all over the temperature range. The insert is zooming of the relaxation process of the signal, which is the field of study of this project as mentioned before. This measurement is done to understand the different transformations of the sample which are principally the following ones:

- Glass transition
- Undercooled liquid
- Crystallisation

Figure 3.15 is in agreement with table 2.1[8]. As it can be seen, the glass state ends roughly at $T_g = 300K$, the crystallisation process starts approximately at $T_x = 400K$ reaching then the crystalline state, consequently between the glass and crystal state the supercooled liquid is found. The exact temperatures are calculated later. Experimentally proving the theoretical part, one can continue with the measurements knowing that the rest of the $Pd_{40}Ni_{40}P_{20}$ cylinder is a glass and the theoretical properties are fulfilled.

[8]Section 2.1.2

3.5 Treatment of the samples

After fabricating the sample as explained in section 3.1, the obtained cylinder of $Pd_{40}Ni_{40}P_{20}$ is cut into pieces with the wire saw. The aim of the project is to study the relaxation process of the material after several deformations. Analyzing the same sample all the time implies that the temperature should not overpass the supercooled liquid region, that is why the measurement will stop at $340°C$ after the glass transition but before crystallisation.

In an ideal case, one can expect that when the first DSC measurement is done the sample can be taken out and reused. After heating the sample until it is completely relaxed, which means that the exponential contribution from the relaxation time tends to zero, the deformation is not present anymore. This process is repeated many times as the number of heating rates desired to investigate, with the objective of studying the appearing signal by Kissinger analyses[9] afterwards. Tables 3.3 and 3.4 show the different masses and heights from each analyzed sample after every process of deformation when the samples are taken out from the DSC; after different processes samples A and B have got different masses and heights all over the experiments. The first measurement, which is an as cast deformed sample, has got the parameters of the second column and the last measurement corresponds to the last column, as exposed in the parameters of tables 3.3 and 3.4. The number of the experiment is given as a number of primes in the exponent of W (Weight) and h (height). The first column is the weight and the height of the sample before being deformed. As it can be observed, the mass changes all over the experiments because when deforming the sample there are some mass losses. This data is useful to calculate the viscosity of the sample. All the measurements are normalized in mass with the aim of having comparable signals.

Sample A

Table 3.3 presents the history of sample A with the respective mass and height during the different measurements at different heating rates and at a cooling rate of 10 K/min. Sample A is deformed by applying HP (High Pressure) with a pressure of 8 GPa, the device is the HPT but no rotations are applied.

[9] Section 4.4

$W(mg)$	$W'(mg)$	$W''(mg)$	$W'''(mg)$	$W'^{v}(mg)$	$W^{v}(mg)$
116.96	116.95	116.89	116.87	116.84	85.31
$h(mm)$	$h'(mm)$	$h''(mm)$	$h'''(mm)$	$h'^{v}(mm)$	$h^{v}(mm)$
0.670	0.670	0.667	0.662	0.660	0.475

Table 3.3: History of sample A

Sample B

Table 3.4 presents the history of sample B with the respective mass and height during the different measurements at different heating rates and at a cooling rate of 10 K/min. Sample B is deformed by applying HPT5 which corresponds to a pressure of 8 GPa and 5 rotations.

$W(mg)$	$W'(mg)$	$W''(mg)$	$W'''(mg)$	$W'^{v}(mg)$	$W^{v}(mg)$
117.42	106.83	90.10	81.45	76.78	71.16
$h(mm)$	$h'(mm)$	$h''(mm)$	$h'''(mm)$	$h'^{v}(mm)$	$h^{v}(mm)$
0.675	0.600	0.533	0.471	0.465	0.447

Table 3.4: History of sample B

Sample C

Table 3.5 shows the different masses and heights from the sample C all over the different measurements at the same heating rate of 20 K/min and at a cooling rate of 10 K/min. Sample C is deformed by applying HPT5.

$W(mg)$	$W'(mg)$	$W''(mg)$	$W'''(mg)$	$W'^{v}(mg)$
110.74	65.68	60.30	51.89	37.51
$h(mm)$	$h'(mm)$	$h''(mm)$	$h'''(mm)$	$h'^{v}(mm)$
0.615	0.470	0.402	0.362	0.329

Table 3.5: History of sample C

As cast samples

Table 3.6 presents the as cast samples with HPT5 applied at different heating rates (indicated in the table) and at a cooling rate of 10 K/min, being W the weight before HPT5 and W' the weight after HPT5.

Heating rate	$W(mg)$	$W'(mg)$	$h(mm)$	$h'(mm)$
20 K/min	110.74	65.68	0.615	0.470
50 K/min	97.67	80.99	0.541	0.476
100 K/min	95.12	72.87	0.605	0.446

Table 3.6: History of the as cast samples[10]

Parameters of tables 3.3 and 3.4

W: As cast sample before deformation
W': As cast after deformation - 20 K/min
W'': After deformation - 20 K/min
W''': After deformation - 10 K/min
W'^{v}: After deformation - 50 K/min
W^{v}: After deformation - 100 K/min

Sample A and B are analyzed in the DSC with the same state for every measurement, by applying the same cooling rate to the sample before the deformation to quench the glass into a comparable state after every cycle of deformation and DSC measurement. At first, the as cast sample is heated at a heating rate of 20 K/min with the method shown in figure 3.16, after the first heating the sample is not as cast anymore, so one can measure again and compare the plots with different heating rates supposing that the sample that comes out from the DSC has every time the same thermal history.

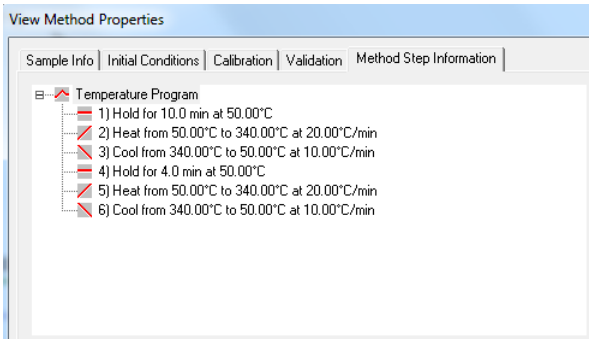

Figure 3.16: Method used in the DSC for a heating rate of 20 K/min

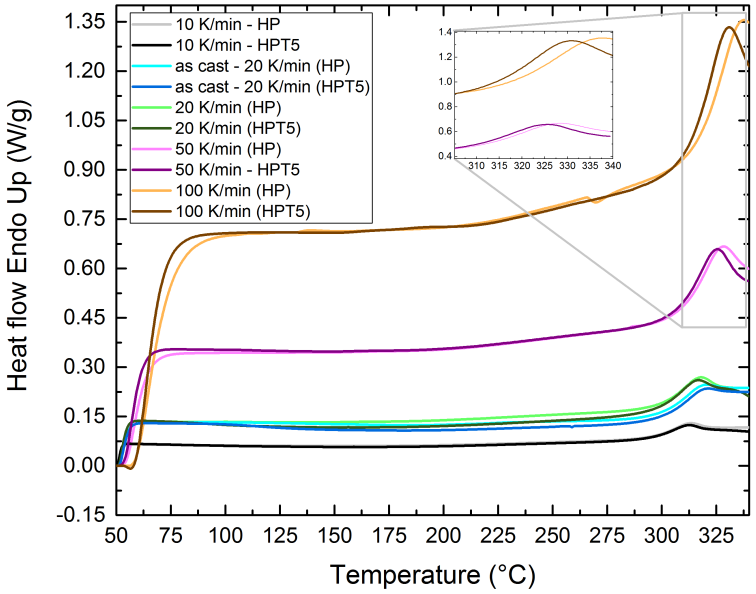

Figure 3.17: Normalized Heat flow vs. Temperature of samples A and B at different heating rates of the first heating cycle

As shown in figure 3.16, at first the sample is held at $50°C$, in order to stabilize the sample and the reference at the same temperature, because the sample is coming from the outside and also because both crucibles should be in argon atmosphere. Afterwards, the second and the third steps are added in order to heat and cool the sample at the exposed

rates; in these experiments the cooling rate will always be 10 K/min and the heating rates will vary with the aim of applying Kissinger analyses.

Figure 3.17 is the plot of the heat flow against the temperature of the first heating cycle in the DSC of sample A corresponding to HP (light colour) and sample B corresponding to HPT5 (dark colour). The range of temperatures in this case goes from $50°C$ to $340°C$. Comparing the first heating cycles with the same heating rates and different deformations (HP and HPT5), one can see that the plot presents a shifting to the right in the endothermic glass transition overshoot when the deformation is HP and to the left when is HPT5, values can be found in tables 3.7 and 3.8.

Heating rate (K/min)	Glass transition peak ($°C$)	$T_{g1/2}$ ($°C$)
20 (as cast)	320.89	306.44
20	317.40	300.65
10	312.80	298.95
50	328.39	312.59
100	337.44	312.80

Table 3.7: Parameters of the first heating cycle after HP with sample A

Heating rate (K/min)	Glass transition peak ($°C$)	$T_{g1/2}$ ($°C$)
20 (as cast)	321.26	307.77
20	316.07	300.95
10	312.10	297.03
50	325.17	308.38
100	330.44	315.06

Table 3.8: Parameters of the first heating cycle after HPT5 with sample B

Table 3.9 contains the values of different deformed as cast sample (HPT5) at different heating rates which will be represented in figure 4.5.

Heating rate (K/min)	Glass transition peak ($^{\circ}C$)	$T_{g1/2}$ ($^{\circ}C$)
20	321.26	307.77
50	319.45	304.03
100	314.52	301.40

Table 3.9: Parameters of the first heating cycle after HPT5 for different as cast samples

In order to compare glass transition temperatures of the samples, it is necessary to study the fictive glass transition temperature[11]. One can suspect that the glass transition temperature will be lower as the deformation is bigger by studying figure 3.17, that is why the fictive temperatures are calculated for three as cast samples and compared with each other (Table 3.10). The values are obtained taking into account different deformations and performing the measurements at the same heating and cooling rates.

Type of deformation applied	T_f ($^{\circ}C$)
Not deformed	310.08
HP	301.08
HPT5	294.75

Table 3.10: Glass transition fictive temperatures for different as cast samples

Table 3.10 shows that T_f decreases as the sample is more deformed. The difference between them is really huge, it is possible to confirm that the supercooled liquid region is less stable as the sample is more deformed.

Viscosity

The viscosity of the samples can be modelled as an exponential decay function. There are several models which can represent the viscosity of the alloy such as the Vogel-Tammann-Fulcher (VTF) equation, the hybrid equation and the free-volume model of Cohen and Grest with their corresponding fit parameters [9]. In this case, the viscosity is studied with the VTF equation which is defined by equation (8).

$$\eta = \eta_1 exp(B/(T - T_0)) \tag{8}$$

[11]Section 3.3

The parameters from equation (8) are: $\eta_1 = 5 \cdot 10^6 Pa \cdot s$, $B = 690K$ and $T_0 = 500K$, which corresponds to the Kauzmann temperature [9]. Taking the glass transition temperature values from tables 3.7, 3.8 and 3.9 and applying equation 8, it is possible to represent the viscosity with respect to the temperature following the VTF equation as shown in figure 3.18 for the different studied samples. The values are fitted with an exponential decay function which is in agreement with the equation (8).

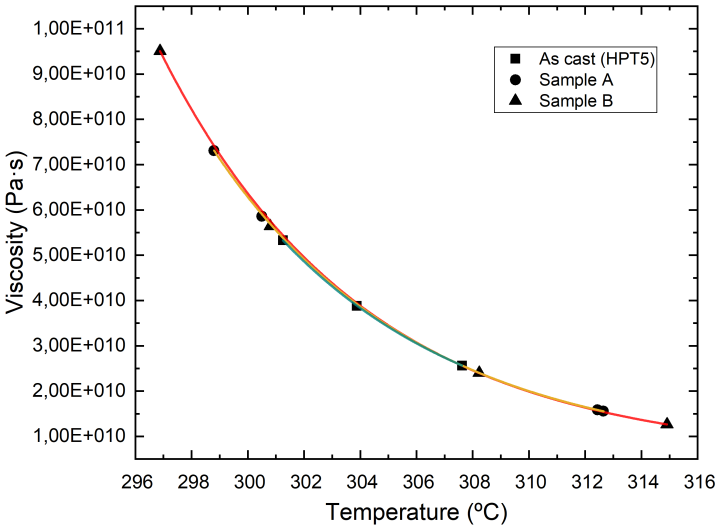

Figure 3.18: Viscosity vs. Temperature for sample A, B and as casts

4 Results & Discussion

4.1 Cooling and heating rates

The method used in the DSC consists of a temperature program with successive steps. The first step is holding the temperature for some minutes before and after each cycle of heating and cooling (figure 3.16), so that the heat flow can be represented with respect to the temperature as explained in section 2.3. In order to choose the right cooling rate for the experimental set up, a sample is analyzed in the DSC by heating at the same heating rate and cooling at different rates as shown in figure 4.1, by doing this the most stable cooling rate can be detected. To have the samples at the same conditions, three heating steps are applied and, in order to see if the reference state is stable, the 2nd and 3rd heating steps from the cooling rate of 20 K/min are subtracted obtaining approximately a 0 line, meaning that the presented system is stabilized.

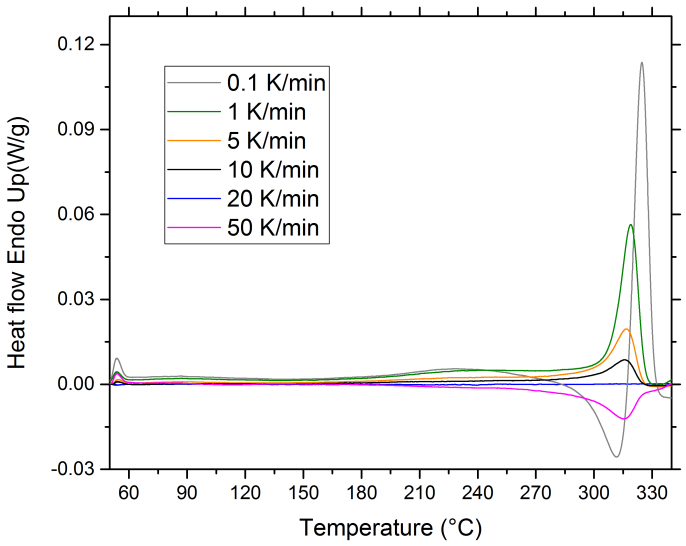

Figure 4.1: Normalized heat flow of PdNiP as cast sample for different cooling rates

Figure 4.1 shows the plot starting at 50°C and ending before crystallization happens, more or less at 340°C at different cooling rates: 0.1 K/min, 1 K/min, 5 K/min, 10 K/min, 20 K/min and 50 K/min. As explained, the reference state in this case is obtained by

vitrifying the sample with a cooling rate of 20 K/min. This reference curve is subtracted from all the plots.

As the cooling rate increases, the peaks observed during the subsequent heating curves are lower and the relaxation parts before glass transition are slightly different. The measurement is done to study how relaxation behaviour is influenced by a variation of different quenching routes. It can be observed that, when the cooling rate is 0.1 K/min, the signal has got endothermic and exothermic parts which could be due to the decreasing in mobility of the particles and the difference in the dynamics of the sample. The exothermic peak at approximately $315°C$ could be due to the rejuvenation of the sample. The chosen cooling rate for the analysis is 10 K/min, because for a higher mass the cooling might be out of control at higher rates; at 10 K/min the state is more defined.

4.2 Stabilization of the sample state

Analysing the parameters and the figures, it seems that applying HPT after every relaxation might have an influence to the following measurements in some way. In order to check how precise the experiments can be, what problems might arise and if the sample has some kind of memory concerning to the analysed heating cycles, the sample B, which was deformed and relaxed several times, is crystallised and compared to the as cast sample without deformation (Figure 4.2). One can expect that the crystallisation of the samples that got through the glass transition should be the same, because all of them come from the $Pd_{40}Ni_{40}P_{20}$ sample and have been completely relaxed upon heating into the undercooled liquid until crystallisation onset.

Figure 4.2 shows the normalized heat flow with respect to the temperature including the crystallisation process of an as cast sample without being deformed (blue), and sample B (orange) after all the suffered deformations and after being annealed. The curves plotted are the result of subtracting the first heating cycles with the second ones from sample B and the as cast sample in order to erase the baseline from both measurements, so the noise from the device affecting the samples is erased.

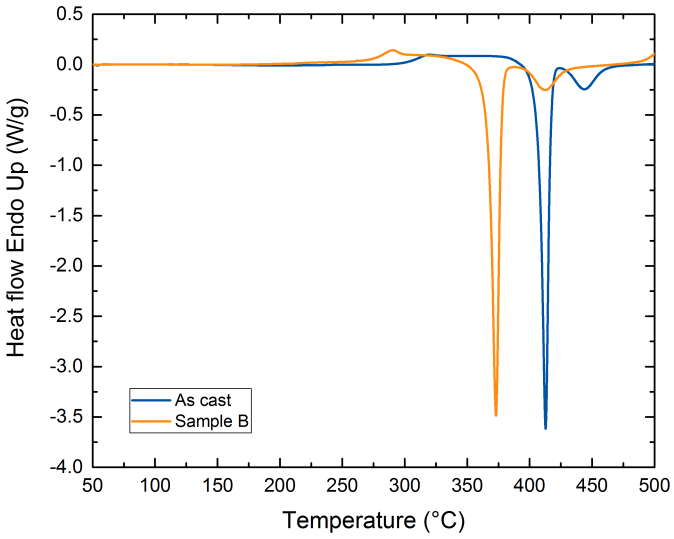

Figure 4.2: Crystallisation process of an as cast sample and Sample B after all the measurements

The as cast sample and sample B show approximately the same behaviour, despite that, they are shifted and they have different T_x differing about $45°C$ from each other, which means that the supercooled liquid is less stable for the sample that has been deformed several times. There are some physical reasons that explain why this is happening: Deforming and annealing several times can induce medium range order in the sample and nucleation sites can be created. The fact that the medium range order (MRO) can be induced, explains why the supercooled liquid of the sample B is not stable. This is why sample B crystallises before the as cast one, these MRO could serve as clusters and act as nucleation sites for the nucleation of the crystalline phase, with a lower barrier than for the nucleation from the completely amorphous sample (i.e. subcritical structures that can become a nucleus).

Calculating the crystallisation enthalpies from the as cast sample and the sample B, one can compare them in order to estimate the crystalline fraction of the sample B. In this case, the as cast sample has got a crystallisation enthalpy of 102.04 J/g and sample B 92.35 J/g. Sample B has lost 10.5% of the crystallisation enthalpy compared to the as cast sample. A small fraction of ΔH is lost over the $\Delta T_x = T_{x\ B} - T_{x\ as\ cast} = 412.80 - 366.60 = 46.20°C$, where T_x are the temperatures at the crystallisation peak. From [10], it is possible to

calculate the δH_{real} as it follows:

$$\delta H_{real} = \delta H_x - \int_{T_{x\ B}}^{T_{x\ as\ cast}} \Delta C_p\, dT = (102.04 - 92.35) - \int_{T_{x\ B}}^{T_{x\ as\ cast}} 0.5895 - 5.143 \cdot 10^{-4} T\, dT$$

$$\delta H_{real} = -1.80\ J/g$$

The obtained result shows that the real difference between crystallisation enthalpies do not differ as much as expected, meaning that there are no crystallites formed during the process and the reduction of the supercooled liquid is due to the changing of MRO.

Finally, it can be possible that a sample after several deformations, even if it is heated up well over T_g, has got some kind of memory which remembers that it was somehow deformed before. This hypothesis can be proved or refused by analysing a sample applying the same process every time, with only one changing variable, which is just the number of deformation and relaxation cycles before the subsequent DSC measurement.

The curve plotted in figure 4.3 is the baseline subtracted heat flow against temperature from sample C at a heating rate of 20 K/min. The measurement was done in order to know if there comes a point where the relaxation part after some measurements has the same contribution and does not differ too much as it differs from the as cast deformed measurement. It is expected that, when the sample is not as cast anymore, the next three subtractions should be the same, but as it can be seen they are not the same at all. Even though the second and the third subtracted heating curves, after the deformed as cast measurement, are more similar than the others, maybe it is due to a saturation state in which the plot can not be shifted to lower temperatures anymore. Figures 4.3 and 4.4 fits to the explanation from the shifting of T_x (Figure 4.2), which means that deformation changes the MRO. Consequently, T_g changes as well and this confirms that the sample is having memory from all the deformation cycles applied during the experiments.

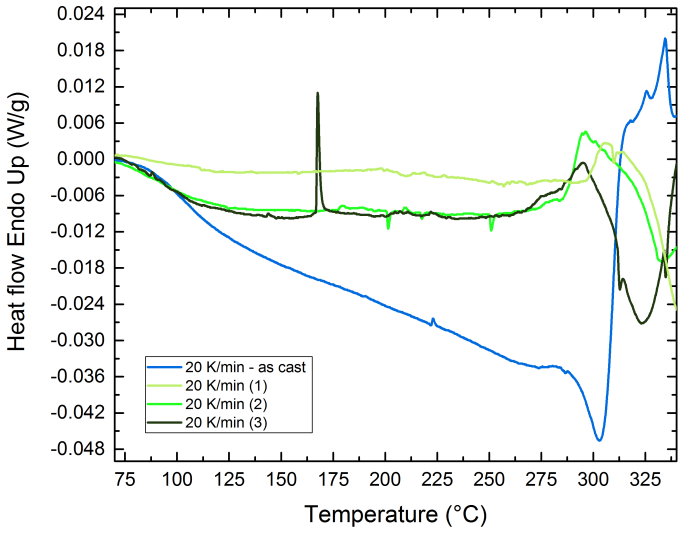

Figure 4.3: Heat flow vs. temperature of the subtraction between 1st and 2nd heating steps (Sample C)

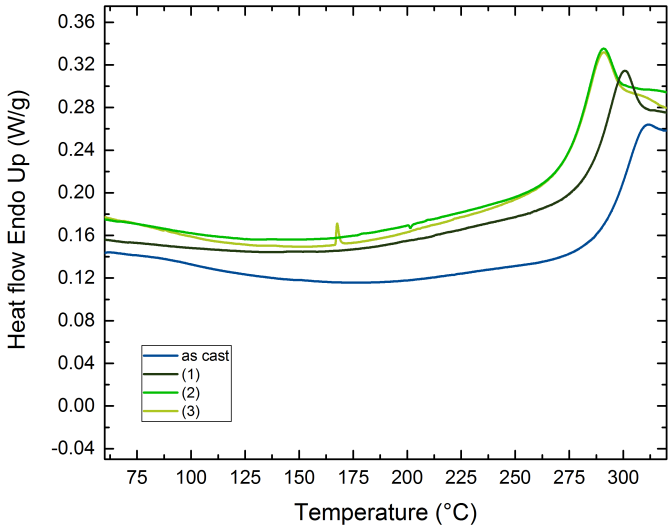

Figure 4.4: Heat flow vs. temperature of the 1st heating step (Sample C)

To see in a better way the reproducibility of the measurements in sample C, figure 4.4 shows the first heating step with the subtracted baseline for each measurement.

From figure 4.3 and 4.4, where the heating rate of each experiment is the same (20 K/min), one can obtain different parameters presented in table 4.1.

Order of the measurement	as cast	(1)	(2)	(3)
Glass transition peak ($°C$)	311.05	300.20	290.40	290.40
T_g ($°C$)	298.44	285.05	276.06	275.09
ΔH_{relax1} (J/g)	13.84	7.24	7.12	7.11
ΔH_{relax2} (J/g)	3.47	7.17	5.05	3.08

Table 4.1: Parameters of sample C

Table 4.1 shows the different parameters from sample C, such as relaxation enthalpies from both heating cycles obtained by calculating the area enclosed in the relaxation process, the glass transition peak from the first cycle and the glass transition temperatures. As seen in figure 4.4, the first measurements have got a higher shifting of the glass transition peak and, after a while, the last measurements are not shifted at all, they seem to stabilize. The parameters from table 4.1 confirms that the glass transition peak at the 3rd and 4th experiment is the same, as well as the glass transition temperature which is almost the same.

One should expect that the values of the parameters and the plots of the different measurements, when they are not as cast anymore, are the same, but the experiments are not like expected. In conclusion, one should be careful with using the same sample for several experiments, because the order of the measurement will matter somehow.

Figure 4.5 shows the subtraction between the first and the second heating cycles of different as cast samples measured at different heating rates. As said before, the samples might have a memory of deformation and relaxation, that is the reason why an analysis for as cast samples is done, so it is comparable with the not as cast ones. As cast samples show more relaxation than the not as cast ones, their enthalpy of relaxation is higher than the one of the not as cast samples and also, as it will be shown in section 4.4, the as cast samples will need slightly more activation energy for relaxation. The information of each as cast sample is written in table 3.6.

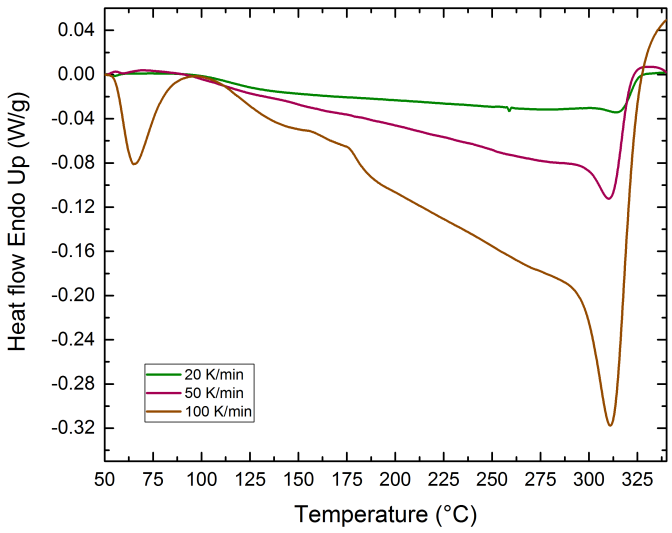

Figure 4.5: Heat flow vs. temperature of the subtraction between the 1st and 2nd heating steps at different heating rates of as cast samples after HPT5

4.3 Data treatment

Figure 4.6 shows the relaxation contribution of the sample due to the different deformations; by subtracting the first and the second heating steps one can remove the quenching contribution from the data. The relaxation enthalpies, defined as the area between the beginning of the measurement and the glass transition zone, are found in tables 4.2 and 4.3.

Heating rate (K/min)	ΔH_{relax1} (J/g)	ΔH_{relax2} (J/g)	Glass transition peak ($°C$)
20 (as cast)	5.54	2.20	314.07
20	7.33	4.55	312.40
10	2.88	2.60	307.10
50	2.77	2.25	324.00
100	3.56	3.05	325.33

Table 4.2: Relaxation enthalpies of the 1st and the 2nd heating cycles and the glass transition peak from the subtraction between both cycles of sample A

Heating rate (K/min)	ΔH_{relax1} (J/g)	ΔH_{relax2} (J/g)	Glass transition peak ($°C$)
20 (as cast)	16.52	5.31	316.07
20	12.13	4.24	314.47
10	4.57	2.13	314.07
50	4.91	3.06	321.84
100	7.27	5.39	331.96

Table 4.3: Relaxation enthalpies of the 1st and the 2nd heating cycles and the glass transition peak from the difference between both cycles of sample B

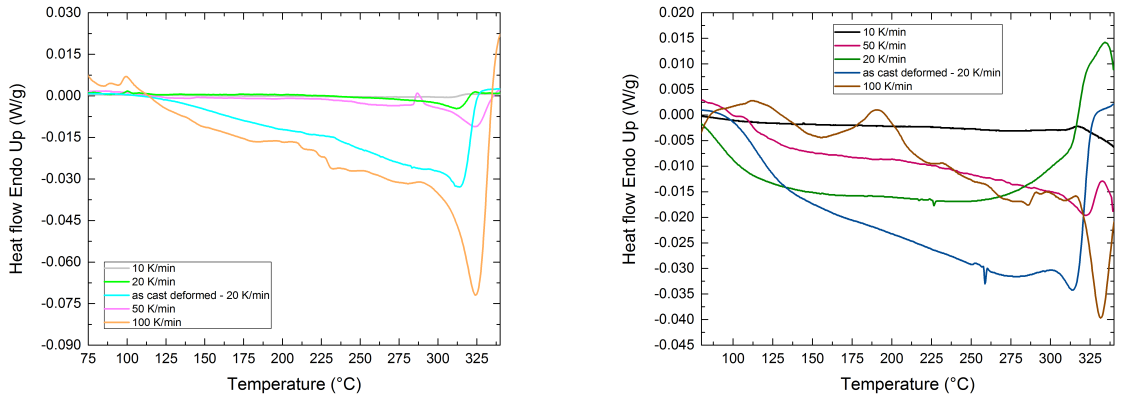

Figure 4.6: Heat flow vs. temperature of the subtraction between the 1st and the 2nd heating steps (2nd step - 5th step from figure 3.16) after HP (left) and HPT5 (right)

Tables 4.2 and 4.3 present the relaxation enthalpies of the first and second heating cycles subtracted with the baseline for each heating rate.

The glass transition peaks are the minimums in the glass transition zones of figure 4.6, which come from the subtraction between both cycles, in such a way that it is possible to know if the subtractions are also shifted for different heating rates. One can prove by observing the tables that when the heating rate increases the subtracted glass transition peak is shifted to the left. The fact that the measurements do not go further than $340°C$ means that it is impossible to make a solid conclusion about why this shifting is occurring, even though the glass transition temperature depends on the experimental cooling and heating rate during measurements [26]. One possible explanation could be that there is a "magnification" effect due to the dependence of the signal on the rate.

4.4 Kissinger Analyses

Theoretical background

Kissinger analyses is a method which makes possible to determine the activation energy for a transformation, regardless of the order of the reaction by making differential thermal analysis patterns at a number of heating rates. When a reaction occurs in DTA (differential thermal analysis), a peak appears indicating a change in enthalpy. A first order reaction has got a variation of the rate with the temperature, the position of the maximum varies with the heating rate if other conditions are fixed. The variation in peak temperature can be used to determine the activation energy [13]. A first order reaction is described as (9).

$$\frac{\partial x}{\partial t} = k(1-x) \tag{9}$$

Where x is the reacted part of the reaction, t the time and k the reaction constant as shown in (10).

$$k = A \cdot e^{-\frac{Q}{RT}} \tag{10}$$

The reaction constant k can be described for a thermally activated process which follows an Arrhenius equation, depending on the activation energy Q, the gas constant R, the constant A and the temperature T. This results in the absolute reaction rate as described in (11).

$$\frac{\partial x}{\partial t} = A(1-x)e^{-\frac{Q}{RT}} \tag{11}$$

Assuming that the signal becomes maximal at a temperature T_{peak} of a measurement with a constant heating or cooling rate $dT/dt = \beta$, one can apply the condition that the derivative of Equation (11) with respect to time equals zero as (12).

$$e^{-\frac{Q}{RT}} = \frac{QA}{R}\frac{\beta}{T_{peak}^2} \tag{12}$$

The activation energy (Q) and the constant A can now be determined from the rate-dependent measurement of T_{peak} by a linear fit $f(x) = b \cdot x + a$ of the logarithmic function (13).

$$-\frac{Q}{RT} = \ln\frac{QA}{R} + \ln\frac{\beta}{T_{peak}^2} \tag{13}$$

By (13), one can define x and f(x) as:

$$x = \frac{-1}{RT_{peak}}$$

$$f(x) = \ln\frac{\beta}{T_{peak}^2}$$

The slope from the linear fit will be the activation enthalpy of the reaction.

Practical application

In this thesis the different relaxation processes indicated by separated minima of the heat flow curve will be analysed to obtain the respective activation enthalpy. By studying the appearing peaks during the relaxation processes of the samples, the processes will be classified as α or β relaxation. The peak positions are obtained as shown in figure 4.7 with the onset option of the Pyris program.

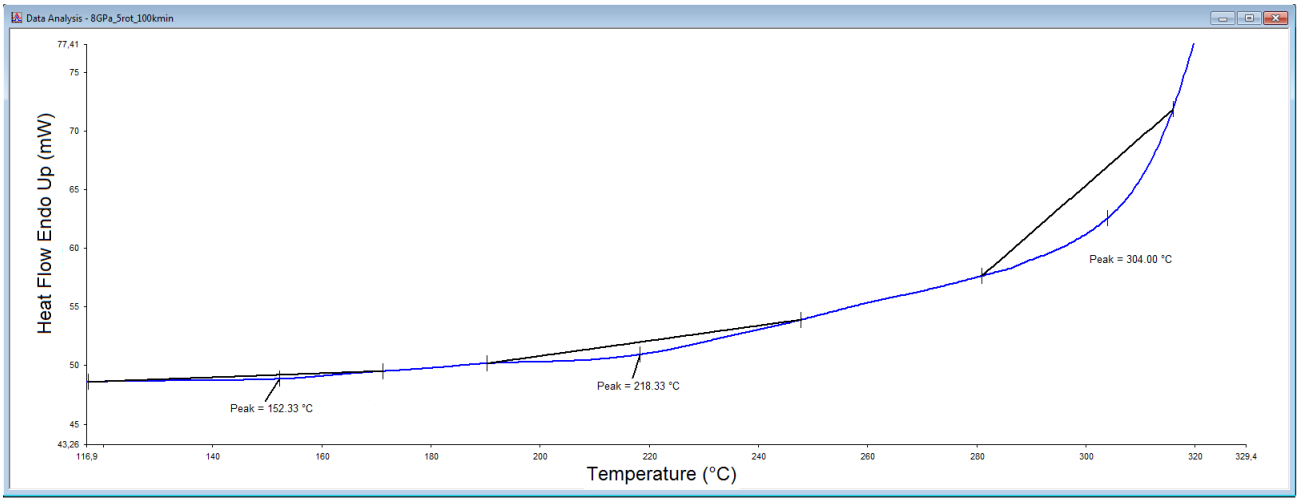

Figure 4.7: Obtained peaks for sample B at a heating rate of 100 K/min (Baseline subtracted)

Tables 4.4, 4.5 and 4.6 present the different values of X and Y (x and f(x) from (13)) with its corresponding peak temperature for samples A, B and as cast at the first heating curve with the subtracted baseline[12]. As explained in section 4.2 with sample C, the third and the fourth time that the sample is deformed and analysed in the DSC somehow stabilises and the heating step is almost the same. Thus, the peaks obtained from the 20 K/min heating rate (deformed as cast and not as as cast) are not taken into account in the Kissinger analyses of sample A and B: they were the first and the second experiments, this means that they correspond to two heating steps that differ more. Kissinger analyses will be more reliable when taking the values from the 3rd experiment until the last one, so the sample in each experiment is behaving the same.

[12]Appendix A

Heating rate (1st peak)	X_1	Y_1	T_{peak} $(^{\circ}C)$
20 K/min	$-3.06 \cdot 10^{-4}$	-8.95 ± 0.03	120 ± 6
50 K/min	$-3.01 \cdot 10^{-4}$	-8.07 ± 0.03	126 ± 6
100 K/min	$-2.93 \cdot 10^{-4}$	-7.43 ± 0.03	138 ± 6
Heating rate (2nd peak)	X_2	Y_2	T_{peak} $(^{\circ}C)$
20 K/min	$-2.73 \cdot 10^{-4}$	-9.18 ± 0.03	167 ± 6
50 K/min	$-2.66 \cdot 10^{-4}$	-8.32 ± 0.03	179 ± 6
100 K/min	$-2.55 \cdot 10^{-4}$	-7.71 ± 0.03	198 ± 6
Heating rate (3rd peak)	X_3	Y_3	T_{peak} $(^{\circ}C)$
20 K/min	$-2.20 \cdot 10^{-4}$	-9.61 ± 0.03	273 ± 6
50 K/min	$-2.17 \cdot 10^{-4}$	-8.72 ± 0.03	280 ± 6
100 K/min	$-2.16 \cdot 10^{-4}$	-8.04 ± 0.03	284 ± 6

Table 4.4: X and Y values for as cast samples

Heating rate (1st peak)	X_1	Y_1	T_{peak} $(^{\circ}C)$
10 K/min	$-3.17 \cdot 10^{-4}$	-9.58 ± 0.03	106 ± 6
50 K/min	$-3.04 \cdot 10^{-4}$	-8.05 ± 0.03	122 ± 6
100 K/min	$-2.96 \cdot 10^{-4}$	-7.41 ± 0.03	132 ± 6
Heating rate (2nd peak)	X_2	Y_2	T_{peak} $(^{\circ}C)$
10 K/min	$-2.84 \cdot 10^{-4}$	-9.79 ± 0.03	150 ± 6
50 K/min	$-2.60 \cdot 10^{-4}$	-8.36 ± 0.03	189 ± 6
100 K/min	$-2.53 \cdot 10^{-4}$	-7.72 ± 0.03	201 ± 6
Heating rate (3rd peak)	X_3	Y_3	T_{peak} $(^{\circ}C)$
10 K/min	$-2.20 \cdot 10^{-4}$	-10.31 ± 0.03	274 ± 6
50 K/min	$-2.09 \cdot 10^{-4}$	-8.79 ± 0.03	301 ± 6
100 K/min	$-2.07 \cdot 10^{-4}$	-8.13 ± 0.03	308 ± 6

Table 4.5: X and Y values for sample A

Heating rate (1st peak)	X_1	Y_1	T_{peak} $(^\circ C)$
10 K/min	$-3.14 \cdot 10^{-4}$	-9.59 ± 0.03	109 ± 6
50 K/min	$-2.98 \cdot 10^{-4}$	-8.09 ± 0.03	130 ± 6
100 K/min	$-2.83 \cdot 10^{-4}$	-7.50 ± 0.03	152 ± 6
Heating rate (2nd peak)	X_2	Y_2	T_{peak} $(^\circ C)$
10 K/min	$-2.66 \cdot 10^{-4}$	-9.92 ± 0.03	178 ± 6
50 K/min	$-2.49 \cdot 10^{-4}$	-8.45 ± 0.03	210 ± 6
100 K/min	$-2.45 \cdot 10^{-4}$	-7.79 ± 0.03	218 ± 6
Heating rate (3rd peak)	X_3	Y_3	T_{peak} $(^\circ C)$
10 K/min	$-2.17 \cdot 10^{-4}$	-10.34 ± 0.03	281 ± 6
50 K/min	$-2.10 \cdot 10^{-4}$	-8.79 ± 0.03	299 ± 6
100 K/min	$-2.08 \cdot 10^{-4}$	-8.11 ± 0.03	304 ± 6

Table 4.6: X and Y values for sample B

The (X,Y) coordinates are represented in figures 4.8, 4.9 and 4.10 and, as Kissinger analyses states, the corresponding slopes will be the activation energies from the relaxation processes.

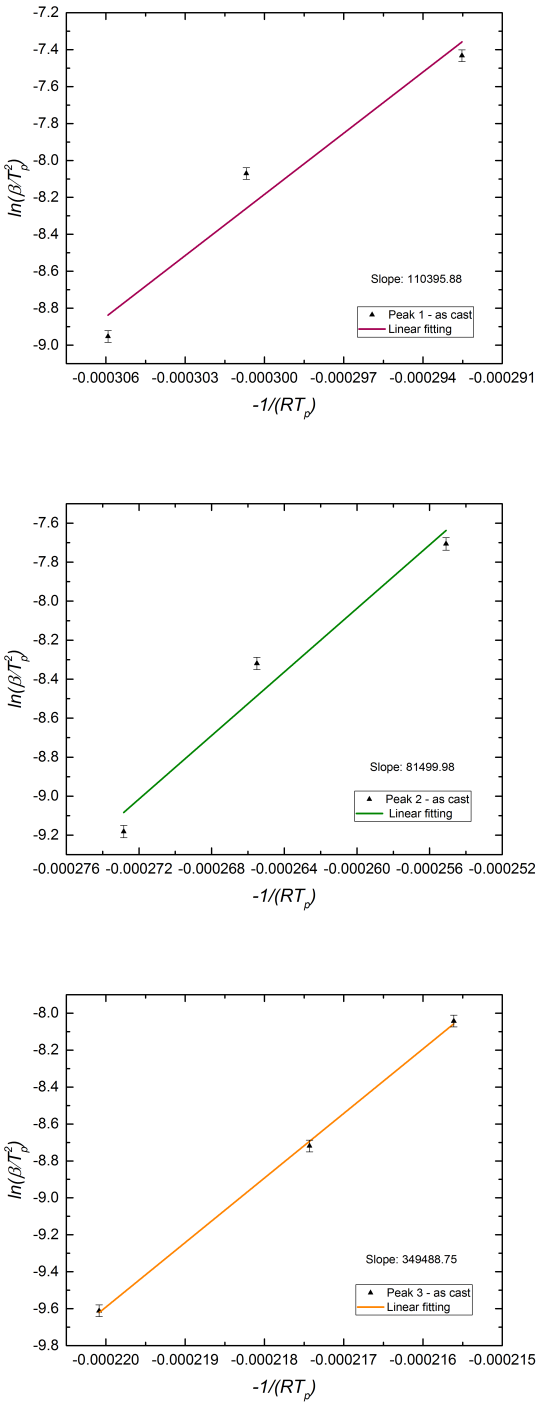

Figure 4.8: Kissinger analyses of the 3 peaks from the as cast deformed (HPT5) samples

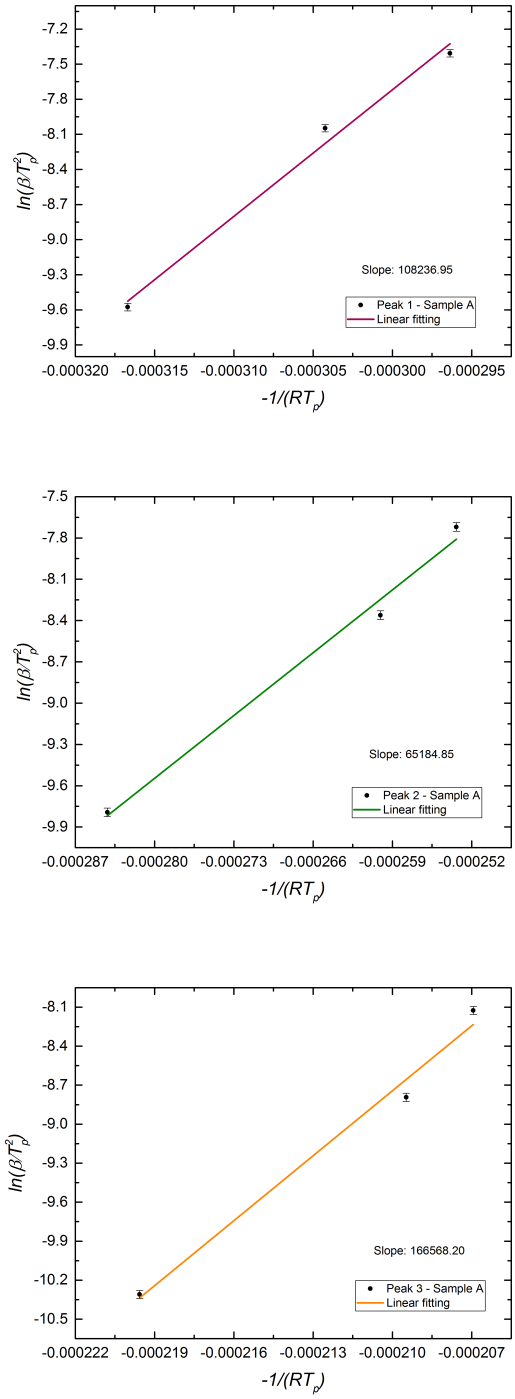

Figure 4.9: Kissinger analyses of the 3 peaks from the not as cast deformed (HP) sample A

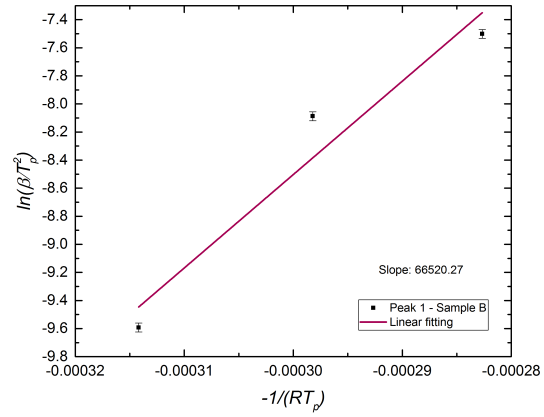

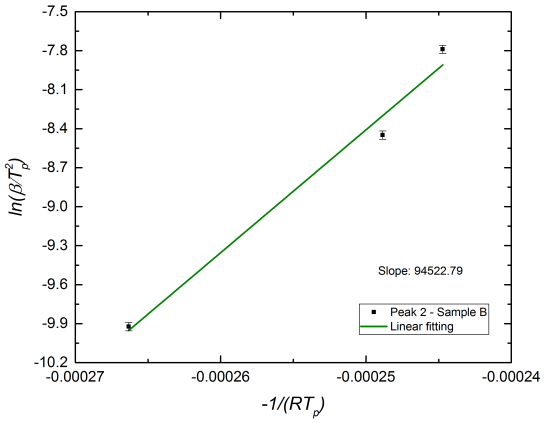

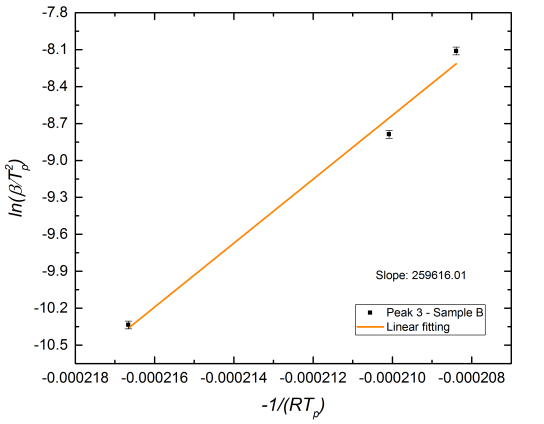

Figure 4.10: Kissinger analyses of the 3 peaks from the not as cast deformed (HPT5) sample B

From figures 4.8, 4.9 and 4.10 the activation enthalpies are obtained by calculating the slope of the different linear functions, these activation enthalpies are presented in tables 4.7, 4.8 and 4.9 for each analyzed sample.

Peak 1	$110 \pm 24\ kJ/mol$
Peak 2	$81 \pm 16\ kJ/mol$
Peak 3	$349 \pm 9.8\ kJ/mol$

Table 4.7: Activation enthalpies for the relaxation processes due to HPT5 and quenching (As casts samples)

Peak 1	$108 \pm 11\ kJ/mol$
Peak 2	$65 \pm 6\ kJ/mol$
Peak 3	$166 \pm 19\ kJ/mol$

Table 4.8: Activation enthalpies (kJ/mol) for the relaxation processes due to HP (Sample A - not as cast)

Peak 1	$66 \pm 16\ kJ/mol$
Peak 2	$94 \pm 12\ kJ/mol$
Peak 3	$259 \pm 28\ kJ/mol$

Table 4.9: Activation enthalpies for the relaxation processes due to HPT5 (Sample B - not as cast)

Table 4.7 present the activation enthalpies for the different relaxation processes from an HPT5 deformed as cast sample, which activation energies are slightly bigger than the ones presented in tables 4.8 and 4.9, that are not as cast samples. The as cast samples have got a contribution in the relaxation part due to quenching and their activation enthalpies are unexpected because the prestructures from the as cast samples are less deformed than sample A or B that have more degrees of freedom.

The relaxation is related to the movement of atoms in different modes which have corresponding activation energies inducing these modes. In principle, relaxation should start earlier in not as cast samples, because some modes are activated before when the sample is as cast. Modes of relaxation might be activated with different heating rates; calculating the relaxation enthalpies applying different heating rates one can see that, for example, at 20 K/min the enthalpy of relaxation is higher than 100 K/min heating, theoretically they should be the same.

The relaxation part which includes the three found peaks is the area in front of the glass transition which can correspond to α-relaxation and β-relaxation. Experimentally, the two relaxation processes are investigated using DSC. The entire exothermic peak is the α-relaxation, which is determined by the β-relaxation. β-relaxation can be assigned to the endothermic peaks. The β-relaxation takes place at lower temperatures before the endothermic fraction. The β-relaxation overlap the signal of the α-relaxation and can not be separated directly from it. The β-relaxation already starts at temperatures below the α-relaxation and it does not contribute in the last peak before glass transition [22]. In conclusion, the exothermic part of the relaxation process correspond to an α-relaxation. The first and the second peaks correspond to α and β relaxation and the third peak only corresponds to α-relaxation.

Nowadays, α and β relaxations are the basis of many studies, since both processes can not be fully explained and there are still many questions to be answered.

Errors

- T_{peak}
  The error is $\pm$ 6°C. It has been calculated by searching the temperature peak in a different range with the Pyris software, observing then that the different values can vary maximum 6°C.

- Y
  The propagated error is calculated by:

  $$\Delta Y = |\frac{df(x)}{dT_{peak}}|\Delta T_{peak} = \frac{2}{T_{peak}}\Delta T_{peak}$$

  The maximum error will be when the temperature peak is the lower one, then for the minimum value of the temperature, one can obtain the maximum error for Y which is $\pm$0.03.

- Activation enthalpies
  The errors from the activation enthalpies correspond to the linear fitting error from the Origin program.

5 Conclusions & Further work

The main objective of this work was to study the calorimetric signals appearing during the relaxation process. By employing the DSC and the Kissinger analyses, their activation energies have been determined so their physical origin could be discussed relating them with their corresponding relaxation type.

During the measurements, one might think that the supercooled liquid region is reduced because samples are partially crystallised after the HPT cycles applied, but it is not true because by TEM it has been proved that these is not the case [23]. Another explanation could be that their MRO is changed, so that is the reason why the samples crystallise before the as cast one. Also, several cycling of deformation and relaxation have an influence on the sample state: the heating cycles are shifted to lower temperatures since they saturate and they have almost the same shape after repeating the experiments two or three times. This means that one cannot suppose that the analysed sample is always the same during all the measurements.

As the sample is deformed and annealed, the glass transition temperature is lower, by these process the samples are submitted to the aging process. Sample A and B have been crystallised and compared to an as cast sample which have not been deformed. It has been proved that their crystallisation enthalpies are lower than the as cast one, implying that the changes of MRO by deformation involve nucleation being more favourable and the decreasing of the enthalpy difference between disordered (amorphous or undercooled liquid) and crystallisation state.

As cast samples have got a bigger contribution in the enthalpy of relaxation and need a bigger activation energy to activate the peaks appearing in the relaxation process, these might be due to the quenching contribution that the as cast samples have in the relaxation process. Samples deformed with the HPT5 need more activation energy in the relaxation peaks than the HP deformed, due to the induction of nucleation sites or due to the induction of MRO.

The exothermic part of the relaxation process correspond to an α-relaxation. The first and the second peaks correspond to α and β relaxation and the third peak only corresponds to α-relaxation.

The applied Kissinger Analyses supposes that the reaction is an Arrhenius type of 1st order, one can not be sure about it and it could be an interesting study to confirm if this assumption is true or not.

Appendix A

Appendix A shows the representations of the normalized heat flow with respect to the temperature. The figures are the first heating steps with the baseline subtracted, divided by the mass and by the heating rate. The sample A shows less relaxation contribution than sample B. Exothermic peaks from Kissinger analyses are taken from these plots.

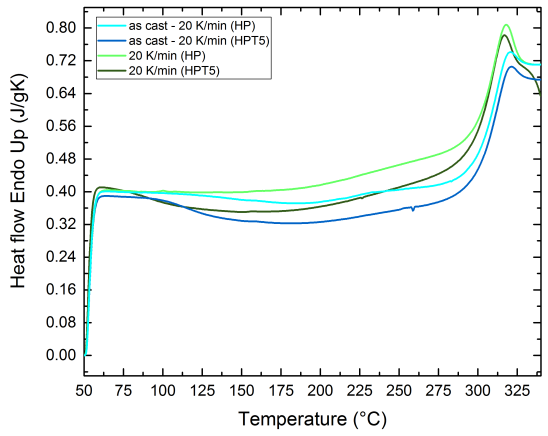

Normalized Heat flow vs. temperature (1st heating step) - 20 K/min

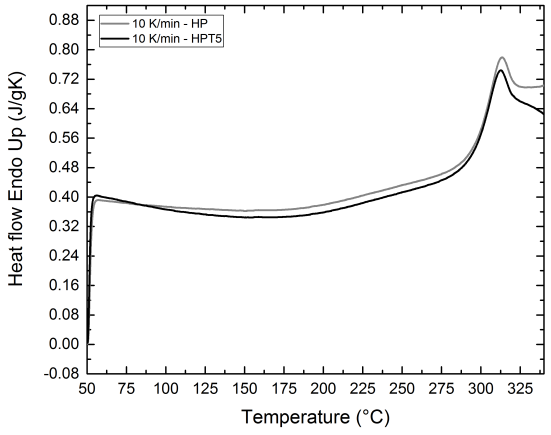

Normalized Heat flow vs. temperature (1st heating step) - 10 K/min

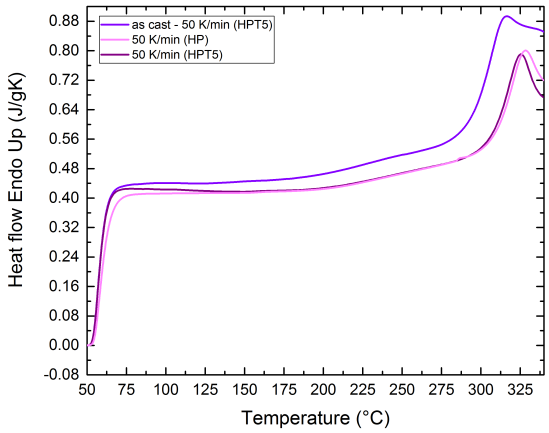

Normalized Heat flow vs. temperature (1st heating step) - 50 K/min

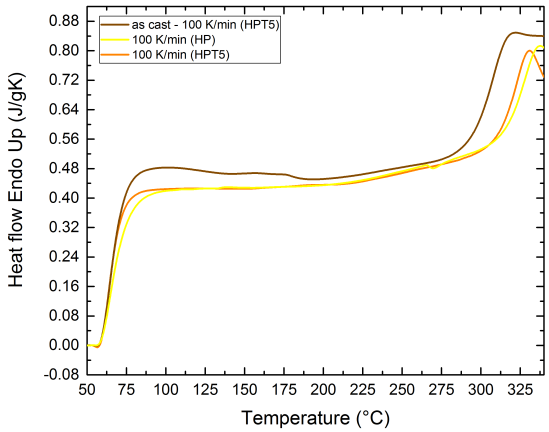

Normalized Heat flow vs. temperature (1st heating step) - 100 K/min

References

[1] A.L. Greer, Y.Q. Cheng, E. Ma. Materials Science and Engineering, Vol. 74, p.71-132, 2013.

[2] A. Slipenyuk und J. Eckert. Correlation between enthalpy change and free volume reduction during structural relaxation of $Zr_{55}Cu_{30}Al_{10}Ni_5$ metallic glass. Scripta Materialia 50, p.39-44, 2004.

[3] B. Dong, S. Zhou, D. Li, C. Lu, F. Guo, X. Ni, Z. Lu. A new criterion for predicting glass forming ability of bulk metallic glasses and some critical discussions. Progress in Natural Science: Materials International 21, p.164-172, 2011.

[4] C. Angell, K.L. Ngai, G.B. McKenna, P. F. McMillan, and S W Martin. Relaxation in glassforming liquids and amorphous solids. Journal of Applied Physics, Vol. 88, N° 6, p.3113-3157, 2000.

[5] E. Rössler, V. N. Novikov, A. P. Sokolov. Toward a general description of the dynamics of glass formers. Phase transitions, Vol. 63, p.201-233 1997.

[6] F.J. Owens, C. P. Poole. The Physics and Chemistry of Nanosolids. John Wiley & Sons, 2008.

[7] G. Gottstein. Physical foundations of materials science. Springer, 2004.

[8] G. Höhne, W. Hemminger, H.J. Flammersheim. Differential Scanning Calorimetry: An introduction for Practitioners. Springer-verlag Berlin Heidelberg GmbH, 1996.

[9] G. Wilde, G.P. Görler, K. Jeropoulos, R. Willnecker and H.J. Fecht. Specific volume, heat capacity and viscosity of a deeply undercooled $Pd_{40}Ni_{40}P_{20}$ bulk glass forming alloy. Materials Science Forum Vols. 269-272, p.541-546, 1998.

[10] G. Wilde, G.P. Görler, R. Willnecker and G.Dietz. Thermodynamic properties of $Pd_{40}Ni_{40}P_{20}$ in the glassy, liquid, and crystalline states. Appl. Phys. Lett, Vol. 65, N°4, p.397-399, 1994.

[11] G. Zschornack. Handbook of X-Ray Data. Springer, 2007.

[12] H. Yu, W. Wang, K. Samwer. The β relaxation in metallic glasses: an overview. Materials Today, Vol. 16, N° 5, p.183-191, 2013.

[13] H. E. Kissinger. Reaction Kinetics in Differenial Thermal Analysis. Analytical chemistry, Vol.29, N°11, p.1702-1706, 1957.

[14] H. H. Uhlig and R. W. Revie, Corrosion and Corrosion Control, 3rd ed. Wiley-Interscience, New York, 1985.

[15] http://www.cas.miamioh.edu/ marcumsd/p293/lab3/lab3.htm (December 2018)

[16] https://www.lenntech.es/tabla-peiodica/radio-atomico.htm (January 2019)

[17] https://www.toppr.com/guides/chemistry/the-solid-state/crystalline-and-amorphous-solids/ (December 2018)

[18] I.R.K. Valiev, R.Z. and I.V. Alexandrov. Bulk nanostructured materials from severe plastic deformation. Progress in Materials Science 45, p.103-189, 2000.

[19] J. Lübke Master's Thesis: Cryogenic Cycling of Bulk Metallic Glasses. A study on thermal and mechanical consequences of thermal cycling. WWM, 2017.

[20] M. Miller, P. Liaw. Bulk metallic glasses. Springer, 2008.

[21] M. Telford. The case for bulk metallic glass. Materials today, Vol.7, p.36-43, 2004.

[22] N. Nollman. Plastische Deformation und mechanische Eigenschaften von Palladium-basiertenmetallischen Gläsern. Dissertation in Physik angefertigt im Institut für Materialphysik. WWM, July 2018.

[23] S.Hilke, private communication.

[24] T. C. Hufnagel, C. A. Schuh, M. L. Falk. Deformation of metallic glasses: Recent developments in theory simulations, and experiments. Acta Materialia 109, p.375-393, 2016.

[25] W. Dmowski, Y. Yokoyama, A. Chuang, Y. Ren, M. Umemoto, K. Tsuchiya, A. Inoue, T. Egami. Structural rejuvenation in a bulk metallic glass induced by severe plastic deformation. Acta Materialia, Vol. 58, Issue 2, p.429-438, 2010.

[26] W.H. Wang, C.Dong, C.H. Shek. Bulk metallic glasses. Materials Science and Engineering R 44, Vol. 44, p.45-89, 2004.

[27] Y. He, R. B. Schwarz, J. I. Archuleta. Bulk glass formation in the Pd–Ni–P system. Appl. Phys. Lett., Vol. 69, No. 13, p.1861-1863, 1996.

Acknowledgements

I would like to thank Prof. Dr. Gerhard Wilde for giving me the opportunity to work in this project, for his expert advice and for taking his time to mentor me. I am also grateful to Prof. Dr. Jordi Llorca for accepting to be my codirector and helping me in everything he could, including the bureaucracy and giving me advices concerning to the project.

I would like to thank in a special way my supervisor Mark Stringe for being so patient when teaching me how devices work, solving doubts and supervising my work, always explaining the reason behind every decision.

I am grateful to my laboratory mates: Aaron, Friederike, Katharina, Lena, Luke, Manoel and Saba for helping me in everything they could, they have been my main support in the department. Finally, I would like to thank my friends for supporting me from Barcelona and Girona, although they still do not know what I am doing in Münster. Thank you.

To my family: Lluís, Eulàlia, Maria, Joan, Andreu, Mercè, Joaquim, Pere, Xavier, Núria and Tomàs.